

NASA TECHNICAL NOTE



NASA TN D-4404

C. 2

NASA TN D-4404



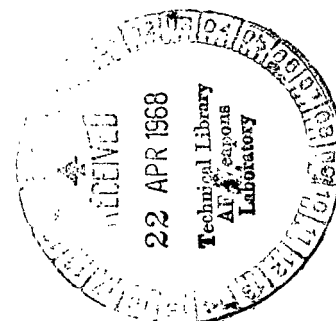
TECH LIBRARY KAFB, NM

LOAN COPY: RETURN
AFWL (WLIL-2)
KIRTLAND AFB, N MEX

AN ANALYSIS OF ENERGETIC SPACE RADIATION AND DOSE RATES

by M. O. Burrell, J. J. Wright, and J. W. Watts

*George C. Marshall Space Flight Center
Huntsville, Ala.*





AN ANALYSIS OF ENERGETIC
SPACE RADIATION AND DOSE RATES

By M. O. Burrell, J. J. Wright, and J. W. Watts

George C. Marshall Space Flight Center
Huntsville, Ala.

NATIONAL AERONAUTICS AND SPACE ADMINISTRATION

For sale by the Clearinghouse for Federal Scientific and Technical Information
Springfield, Virginia 22151 - CFSTI price \$3.00

TABLE OF CONTENTS

	Page
SUMMARY	1
INTRODUCTION	1
RADIATION DOSE CALCULATIONS AND DEFINITIONS	2
THE GEOMAGNETIC FIELD AND CHARGED PARTICLE INTERACTIONS.	6
GALACTIC COSMIC RADIATION	11
SOLAR COSMIC RADIATION	13
PREDICTION OF SOLAR PROTON EVENTS.	25
TRAPPED PROTONS	28
TRAPPED ELECTRON AND BREMSSTRAHLUNG RADIATION	38
SYNCHRONOUS ORBIT RADIATION	46
CONCLUSIONS	50
APPENDIX	51
REFERENCES	56

LIST OF ILLUSTRATIONS

Figure	Title	Page
1.	Monoenergetic Proton Dose as a Function of Depth Penetrated for Various Source Energy Spreads	5
2.	Recent Satellite Version of the Magnetosphere Based on Results of IMP-1 Magnetic Field Experiment (November 27, 1963, to May 31, 1964)	7
3.	The Geometry of the B-L Coordinate System	8
4.	Rigidity as a Function of Kinetic Energy for Protons and Alpha Particles	10
5.	Variation of Proton Vertical Cutoff Energy During a Solar Active Period and as a Function of Earth Radii and Latitude During Quiet Time	11
6.	Galactic Cosmic Ray Differential Energy Spectra and Dose Rates Behind Aluminum Shields.	12
7.	Total Cosmic Ray Proton Dose Rate as a Function of Orbital Inclination	13
8.	Typical Intensity-Time Profiles During a Solar Cosmic Ray Event	14
9.	Total Proton Skin Dose Behind Aluminum Shields for Several Solar Flares	17
10.	Total Proton Blood Dose Behind Aluminum Shields for Various Solar Cosmic Ray Events	18
11.	Total Proton Skin Dose Behind Polyethylene Shields for Seven Large Solar Cosmic Ray Events	20
12.	Modified Differential Energy Spectrum and Corresponding Dose for the November 12, 1960, Solar Flare	22
13.	Comparison of Total Proton Skin Dose Using Masley and Webber Spectra	23
14.	Total Proton Skin Dose Behind Aluminum Shields for Various Characteristic Rigidity Values	24
15.	Characteristic Rigidity as a Function of Proton-to-Alpha Ratio	24

LIST OF ILLUSTRATIONS (Continued)

Figure	Title	Page
16.	A Comparison of Proton and Alpha Ray Skin Dose as a Function of Aluminum Shield Thickness	25
17.	Distribution of the Integrated Flux Per Event as a Function of the Number of Events for Solar Cycle 19	27
18.	Monthly Probability of a Proton Event as a Function of Event Size	27
19.	Cumulative Probability Distributions for 2 and 52 Week Missions as a Function of Dose for Various Shield Thicknesses	29
20.	Doses Received on 2 and 52 Week Missions as a Function of Shield Thickness for Various Cumulative Probabilities	30
21.	Trapped Omnidirectional Proton Flux Above 4 and Above 15 MeV	31
22.	Trapped Omnidirectional Proton Flux Above 34 and Above 50 MeV	32
23.	Low Altitude Total Proton Dose Rate as a Function of Shield Thickness and Altitude for 0- and 30-Degree Orbital Inclinations	33
24.	Low Altitude Total Proton Dose Rate as a Function of Shield Thickness and Altitude for 60- and 90-Degree Orbital Inclinations	34
25.	Total Proton Dose Rate as a Function of Shield Thickness and Altitude for 0- and 30-Degree Orbital Inclinations	35
26.	Total Proton Dose Rate as a Function of Shield Thickness and Altitude for 60- and 90-Degree Orbital Inclinations	36
27.	Proton Isoflux Plot at an Altitude of 400 km in the South Atlantic Anomaly	37
28.	Integral Proton Flux Received on a 30-Degree Circular Orbit at an Altitude of 240 Nautical Miles	37
29.	Projected Electron Environment for December 1968	39

LIST OF ILLUSTRATIONS (Continued)

Figure	Title	Page
30.	Projected Electron and Bremsstrahlung Dose Rate as a Function of Altitude and Shield Thickness for 0-Degree Orbital Inclination	40
31.	Projected Electron and Bremsstrahlung Dose Rate as a Function of Altitude and Shield Thickness for 30-Degree Orbital Inclination	41
32.	Projected Electron and Bremsstrahlung Dose Rate as a Function of Altitude and Shield Thickness for 60-Degree Orbital Inclination	42
33.	Projected Electron and Bremsstrahlung Dose Rate as a Function of Altitude and Shield Thickness for 90-Degree Orbital Inclination	43
34.	Electron and Bremsstrahlung Dose Rate as a Function of Shield Thickness Using a Typical Electron Integral Spectrum	44
35.	Electron and Bremsstrahlung Dose Rate as a Function of Shield Thickness for Several Characteristic E_o Values . . .	45
36.	Synchronous Orbit Integral Electron Flux as a Function of Local Time	47
37.	Synchronous Orbit Electron and Bremsstrahlung Dose Rate as a Function of Shield Thickness and Local Time . . .	48
38.	Synchronous Orbit Electron and Bremsstrahlung Dose Rate Using an Average Electron Spectrum	49
39.	Trapped Electron Flux for Circular Orbits as a Function of Altitude and Orbital Inclination.	51
40.	Electron and Bremsstrahlung Dose Rate as a Function of Altitude and Shield Thickness for 0-Degree Orbital Inclination	52
41.	Electron and Bremsstrahlung Dose Rate as a Function of Altitude and Shield Thickness for 30-Degree Orbital Inclination	53

LIST OF ILLUSTRATIONS (Concluded)

Figure	Title	Page
42.	Electron and Bremsstrahlung Dose Rate as a Function of Altitude and Shield Thickness for 60-Degree Orbital Inclination	54
43.	Electron and Bremsstrahlung Dose Rate as a Function of Altitude and Shield Thickness for 90-Degree Orbital Inclination	55

LIST OF TABLES

Table	Title	Page
I	Radiation Dose Limits for 30 - 60-Day Missions	4
II	Integral Proton Flux (Protons/cm ² -Flare) at 30 and 100 MeV with Corresponding Characteristic Rigidity P ₀ and N ₀	16
III	Total Estimated Solar Flare Doses by Event for Ten Shielding Configurations	19
IV	Total Estimated Solar Flare Dose Behind Polyethylene Shields	21

AN ANALYSIS OF ENERGETIC SPACE RADIATION AND DOSE RATES

SUMMARY

The results presented in this report should be of practical value for preliminary engineering analysis of space hazards and planning of possible space missions for either near-earth orbits or deep-space probes. The dose rate curves shown in this report are based on the latest environmental analysis by NASA and the United States Air Force. The environmental models and data are continually updated as experimental data improves and as more sophisticated analyses are performed. As such modifications become available, the authors of this report intend to update the radiation dose rates in future reports.

INTRODUCTION

This study is intended to present a compendium of the environmental data on trapped and untrapped radiation. It considers the calculated tissue dose rates received from these radiations and the induced secondary radiation behind various shield thicknesses. Energetic radiation, as used here, refers to particles with energies greater than about 0.5 MeV. The results given in this report should be of practical value for preliminary analysis of the radiation hazard to man during space flight.

The radiation environment consists of protons and electrons in the Van Allen belts, energetic solar radiation, and galactic cosmic radiation. The solar wind is not included in this study since no appreciable dose is received behind any nominal shielding.

The environmental data used in this report was taken primarily from the works of J. I. Vette of NASA/Goddard Space Flight Center and W. R. Webber of the Boeing Company.

RADIATION DOSE CALCULATIONS AND DEFINITIONS

In this report the radiation dose rate calculations are based on the physical property of energy deposition at a tissue point detector located at the center of a spherical shell of aluminum or polyethylene. The units of dose are in rads-tissue. By definition the rad is the physical equivalent of an energy deposition of 100 ergs/g (0.01 J/kg). The assumption of a tissue point detector is an oversimplification and always leads to a high estimate of the true dose. When skin dose is used, the above conditions of a point detector at the center of a spherical shell with no self-shielding by the target should be specified. Thus, if an astronaut is placed at the point detector location he would receive considerable self-shielding from the rest of his body. In general, the skin doses should be about a factor of two lower on a man target than shown in the curves of this report. (This will also apply to depth doses at 5 cm or less inside the man.) In the present report depth doses were derived when a sphere of tissue was placed about the point detector; the depth indicates the radius of this sphere.

In this work the presented proton dose rate calculations include both primary protons and associated secondary particles. The secondary particle dose component for thin shields can be approximated fairly well by ignoring the attenuation of the primary flux because of inelastic collisions [1].

The units of shield thickness throughout this report are given in grams per square centimeter, which may be converted to centimeters by dividing this thickness by the material density (g/cm^3). For example, aluminum $\rho = 2.7 \text{ g}/\text{cm}^3$; thus, $2.7 \text{ g}/\text{cm}^2$ of aluminum is one centimeter thick. The use of grams per square centimeter thickness has historical precedence in charged particle transport calculations and indeed is quite convenient for two reasons. First, in terms of this unit the penetration characteristics of charged particles are almost the same in all materials (hydrogen is the only exception); second, the mass or weight of a shield can be found for a simple geometry by multiplying the shield thickness by the surface area of the shield.

The most important question that arises in the radiation area is the number of rads that a man, photographic film, or instrument can receive before damage is caused or detected. Of course, this is not always an easy question to answer. For example, very fast film may be damaged beyond feasible use after a one-rad exposure, whereas other films may tolerate 50 or more rads. Thus, each film type has to be investigated regarding its use and possible radiation exposure. Most electronic devices can tolerate very large doses before serious degradation of performance results. Such doses will not be encountered from

natural space radiations for periods of less than one year if the device is behind a shield of one centimeter of aluminum. Solar panels and thermal coatings on spacecraft may be damaged by the large surface doses they receive from low energy electrons and protons.

If man is involved in space flight, his safety from radiation damage should be the first consideration. The following outline of human responses to an exposure in rads is given as a guide [2]. Such a memorandum, of course, cannot be considered as an official NASA document, but it is felt by the authors to reflect the extent of the radiation problem better than a table of acceptable dose levels:

- A. Gastrointestinal dose - The dose required to produce nausea in 10 percent of the crew = 25 rads.
- B. Skin dose - The dose required to produce erythema in 10 percent of the crew (may produce temporary loss of hair) = 200 rads.
- C. Hematological dose - The dose required to produce a 20 percent depression of leukocytes and/or thrombocytes = 50 rads.
- D. Eye dose - The dose required to produce a 5 percent incidence of clinically significant cataracts = 80 rads.

The writers of this memorandum suggested that the "Planning Operational Dose" should be exactly one-half the above outlined doses at the various locations in the body. The "Maximum Operational Dose" is that given above. The radiation exposure levels were selected according to the following operational criteria:

Planning Operational Dose (POD): The dose which should not be exceeded without requiring a mission modification of some degree. The degree of modification will be a function of the magnitude of the excess dose and will be formulated by mission rules. This dose will be used for mission planning purposes to determine if proposed trajectories and time lines are acceptable.

Maximum Operational Dose (MOD): The dose which should not be exceeded without specific modification of the mission to prevent further radiation exposure. Such an exposure would be considered to result in a potentially harmful inflight response in terms of crew safety and post-flight response in terms of delayed radiation injury.

Of course, many factors enter into the determination of the accumulated radiation dose that a man can safely receive. For example, if he received a 25-rad gastrointestinal dose over a two-year period the effects will be much less pronounced than the effect of receiving the same dose over a two-week period. Therefore, the above listing of human responses refer to fairly short term exposures where the human organism has not been capable of significant biological repairs.

The following doses [3] are established on the assumption that the crew will be exposed to small increments of dose on each orbit. No allowance is made for pulses of radiation received at higher intensities. Table I should not be used for missions of longer duration than 60 days.

TABLE I. RADIATION DOSE LIMITS FOR 30 - 60-DAY MISSIONS

Tissue	Depth	P O D	M O D
Skin	0.1 mm	2.5 rads/day	5 rads/day
Eye	3.0 mm	1.25 rads/day	2.5 rads/day
Bone Marrow	5.0 cm	0.6 rad/day	1.0 rad/day

If one wishes to investigate missions of long duration (one or two years) he may assume that the body does indeed repair some of the damage; however, it would be presumptuous to extend the acceptable dose levels without more knowledge. It is conceivable that a total allowable accumulated dose may in fact be doubled for a mission of one or two years. Such an assumption, however, must embody the concept of a fairly constant or uniform radiation exposure over the total period. This is probably not a valid assumption for deep space flight since one could conceivably receive 90 percent of his allowable dose during one large solar proton event lasting (at most) three days.

It is quite valid to inquire if there has been experimental verification of the radiation dose computational methods. The basic parameters for proton and electron transport in matter (range and stopping power data) have been frequently measured experimentally and are quite valid. These basic data, however, are only the building blocks of the much more involved dose rate calculations.

The experimental verification of proton dose rate calculations, for example, is not easily obtained for several reasons. Laboratory proton sources are usually monoenergetic, whereas flare sources have continuous energy spectra. Also, when a theoretical computation is made for a monoenergetic source, the energy band is depicted as a monoenergetic line; whereas in the experiment the proton beam may have a 5 percent energy spread. This energy spread in the source may have a much greater effect on the attempt to duplicate a theoretical result than is commonly believed. Figure 1 illustrates the differences in proton energy deposition in tissue and aluminum for three different energy spreads about a nominal energy of 100 MeV. The source was taken as 10^8 protons/cm² uniformly distributed in the energy band $100 \pm \Delta E$. The spiked curve was obtained by using an energy spread of only ± 0.005 MeV. This type of curve is characteristic of a theoretical calculation, whereas the other curves of Figure 1 are typical of experimental results. The only effect considered in these calculations was an energy spread in the source.

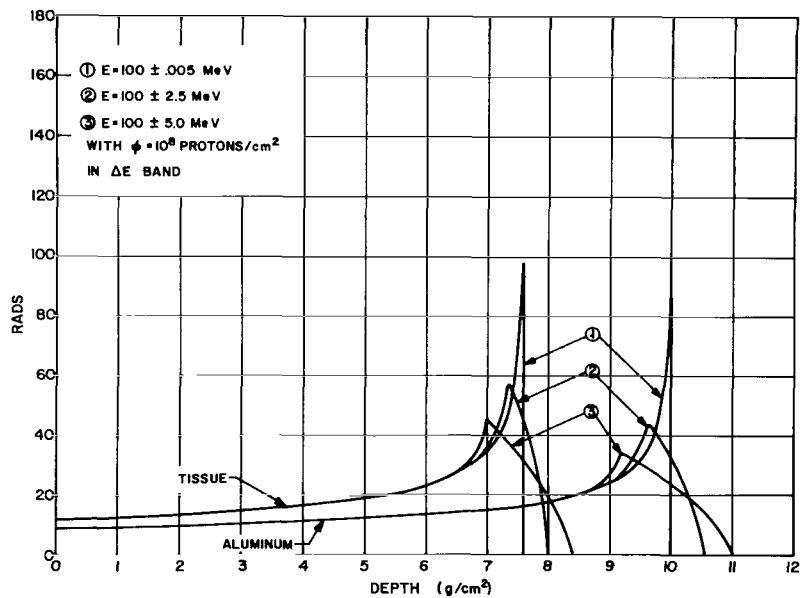


FIGURE 1. MONOENERGETIC PROTON DOSE AS A FUNCTION OF DEPTH PENETRATED FOR VARIOUS SOURCE ENERGY SPREADS

In conclusion, the writers would like to warn against the indiscriminant use of the parametric curves presented in this study. The dose rates in general should be halved in order to obtain the proper dose rate on an astronaut or on other fairly large targets. Also, since actual spacecraft configurations are not spherical shells, an additional reduction in dose (as much as a factor of two) will be found if a realistic geometric representation is used in which shielding from onboard components, other astronauts, and outside structures are considered. For very thin walled structures such as in the S-IVB workshop, such improvements may be very significant. For a more detailed discussion on the radiation transport methods, see References 1 and 4.

THE GEOMAGNETIC FIELD AND CHARGED PARTICLE INTERACTIONS

The geomagnetic field around the earth forms a "magnetic pocket" known as the magnetosphere. The boundary of the magnetosphere is determined by the solar wind which is assumed to be a radial expansion of the sun's corona. At a certain radial distance above the earth, the geomagnetic field energy density equals the energy of the solar wind and there is a breakdown of the magnetic lines of force. This turbulent region is the magnetospheric boundary or transition zone. In the magnetosphere the magnetic field dominates, while outside the magnetosphere, the solar wind is the controlling energy mechanism.

The inner boundary of the transition region, called the magnetopause, occurs at about ten earth radii on the sunlit side of the earth, while the outer boundary of the transition region is in the form of a shock wave at about fourteen earth radii. The magnetopause around the earth is in the form of an elongated teardrop with a long tail pointed away from the sun. Figure 2, taken from Ness [5], shows a recent version of the magnetosphere.

Perhaps the best way to represent the distribution of magnetically trapped particles about the earth is by using the B-L coordinate system developed by Carl McIlwain [6]. The B coordinate denotes the magnetic field strength at some specified point in space; L is the magnetic shell parameter that labels the shell upon which the guiding center of the trapped particle is adiabatically confined as it drifts around the earth. The L coordinate is approximately constant along a geomagnetic field line. In a dipole field, L is constant along the field line and has the geometric property of being the equatorial distance from the dipole center to the magnetic field line. The geometry of the B-L coordinate system is

RESULTS OF IMP-1 MAGNETIC FIELD EXPERIMENT (11/27/63 TO (5/31/64)

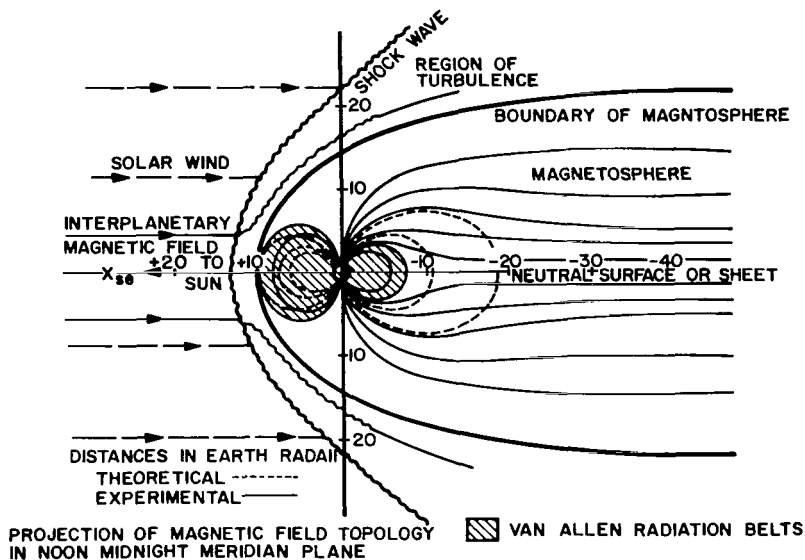


FIGURE 2. RECENT SATELLITE VERSION OF THE MAGNETOSPHERE
 BASED ON RESULTS OF IMP-1 MAGNETIC FIELD EXPERIMENT
 (NOVEMBER 27, 1963, TO MAY 31, 1964)

depicted in Figure 3. For a dipole field the B-L coordinates are related to the latitude and altitude of a point above the earth by the following:

$$B = \frac{M}{R^3} \left(4 - \frac{3R}{L} \right)^{\frac{1}{2}}, \quad L = \frac{R}{\cos^2 \lambda} \quad (1)$$

where M is the magnetic dipole moment ($0.311653 \text{ gauss } R_e^3$), R is the distance in earth radii units from the center of the earth, λ is the geomagnetic latitude, and R_e is the radius of the earth. These relations should be used with caution since the earth's field cannot be depicted as a simple dipole. If the magnetic

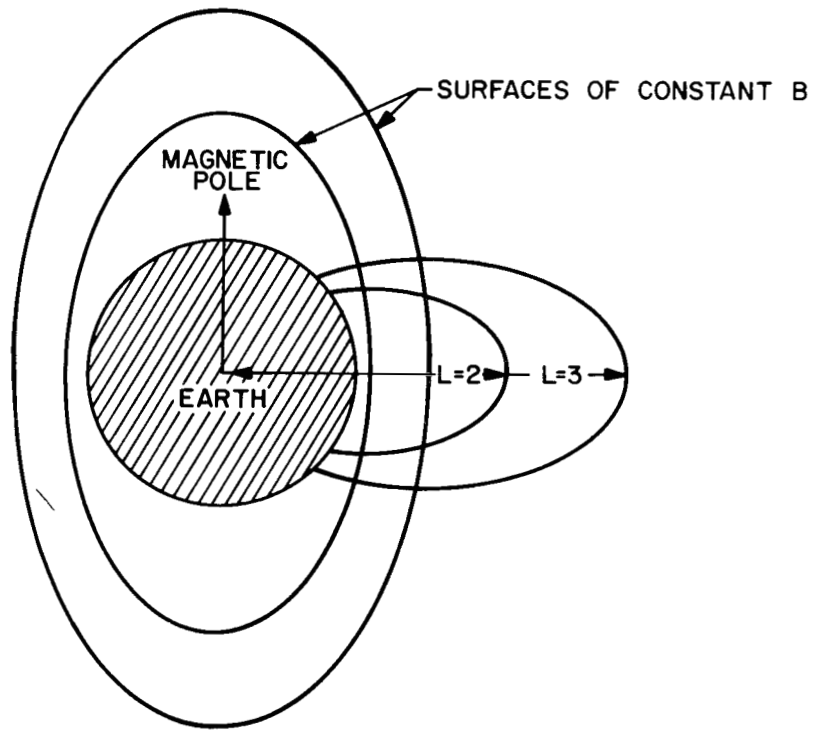


FIGURE 3. THE GEOMETRY OF THE B-L COORDINATE SYSTEM

dipole approximation is used, it should be represented by the more accurate tilted and translated dipole instead of the centered dipole.

The magnetic field of the earth alters the penetration of charged particles to the vicinity of the earth. The theory of the allowed cone of incident charged particles, as developed by Störmer [7], can be used as a basis for calculating the modification of an incoming energy spectrum of cosmic rays or solar flare protons. The theory is based on a dipole approximation of the geomagnetic field. The allowed cone is defined by:

$$p = \frac{60 \times 10^3 \cos^4 \lambda}{R^2 (1 + \sqrt{1 - \cos^3 \lambda \cos \gamma})^2} \quad (2)$$

where R and λ are defined as in equation (1); p is the magnetic rigidity (momentum/charge) in megavolts (MV units); and γ is the half angle of the allowed cone about the normal to the meridian plane [8]. The angle of the allowed cone varies with the energy of the particle and with the position of the observation point [9]. The modified energy spectrum inside the magnetosphere is found by multiplying the external spectrum by the solid angle fraction of the allowed cone as a function of the particle energy.

A computer code has been developed by J. J. Wright to calculate the time weighted modified energy spectrum on any feasible earth orbit by varying the energy (angle) over the allowed cone and weighting each energy (angle) by the time spent at each position in orbit*. The modified energy spectra for galactic cosmic rays and for the November 12, 1960, solar flare will be shown in the following two sections. Shadowing effects of the earth were not considered in these cases. The magnetic rigidity in MV is related to the kinetic energy E in MeV of the particle as follows:

$$p(E) = \frac{\sqrt{E^2 + 2ME}}{q} \quad (3)$$

where q is the total charge, M is the particle rest mass energy (MeV), and E is expressed in MeV.

Equation 3 is plotted in Figure 4 for proton and alpha particles. For $E \leq 100$ MeV, $p \approx \sqrt{2ME}/q = 43.5 \sqrt{E}$, and for $E \geq 10^5$ MeV, $p \approx E/q$.

* For a discussion of methods see reference [10].

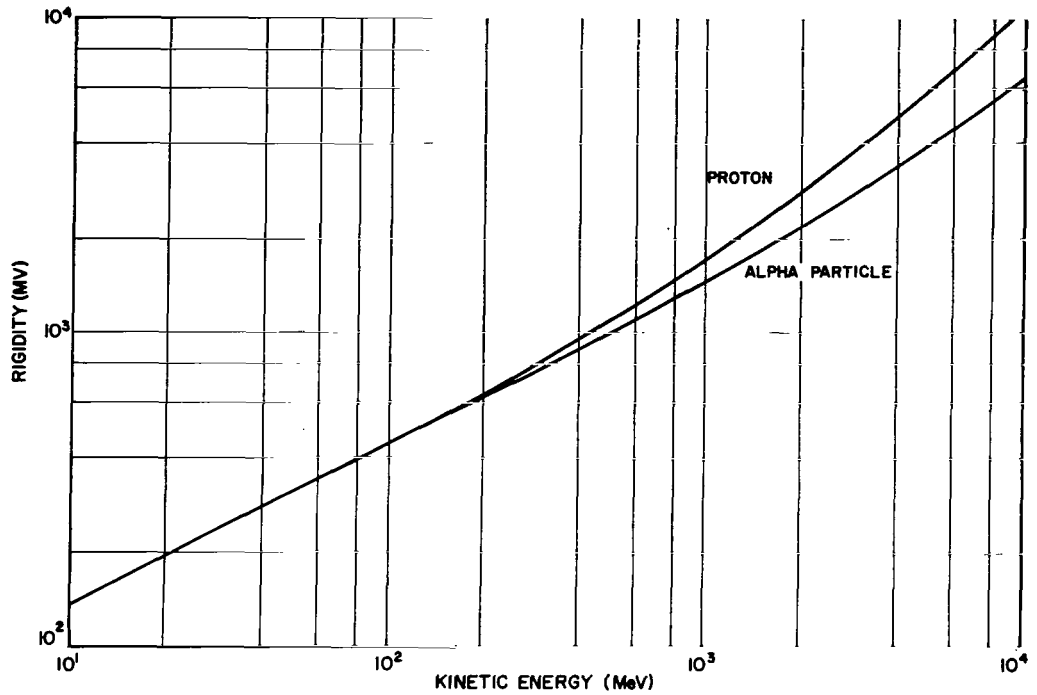


FIGURE 4. RIGIDITY AS A FUNCTION OF KINETIC ENERGY FOR PROTONS AND ALPHA PARTICLES

Combining equations (1), (2), and (3) for $\gamma = 90^\circ$, and solving for the kinetic energy E (MeV), the vertical cutoff energy for protons is found to be

$$E_c = -938 + \sqrt{(938)^2 + \frac{2.25 \times 10^8 \cos^8 \lambda}{R^4}} \quad (4)$$

The so-called vertical cutoff energy signifies that particles coming from the zenith and having energies greater than E_c will intercept a given point (R, λ) .

Figure 5 shows the variation of the vertical cutoff during solar active periods and quiet time [9]. A plot of the proton vertical cutoff energy is also shown in Figure 5 for various earth radii and latitudes for quiet times. The trapped radiation belts will be discussed further in later sections of this report.

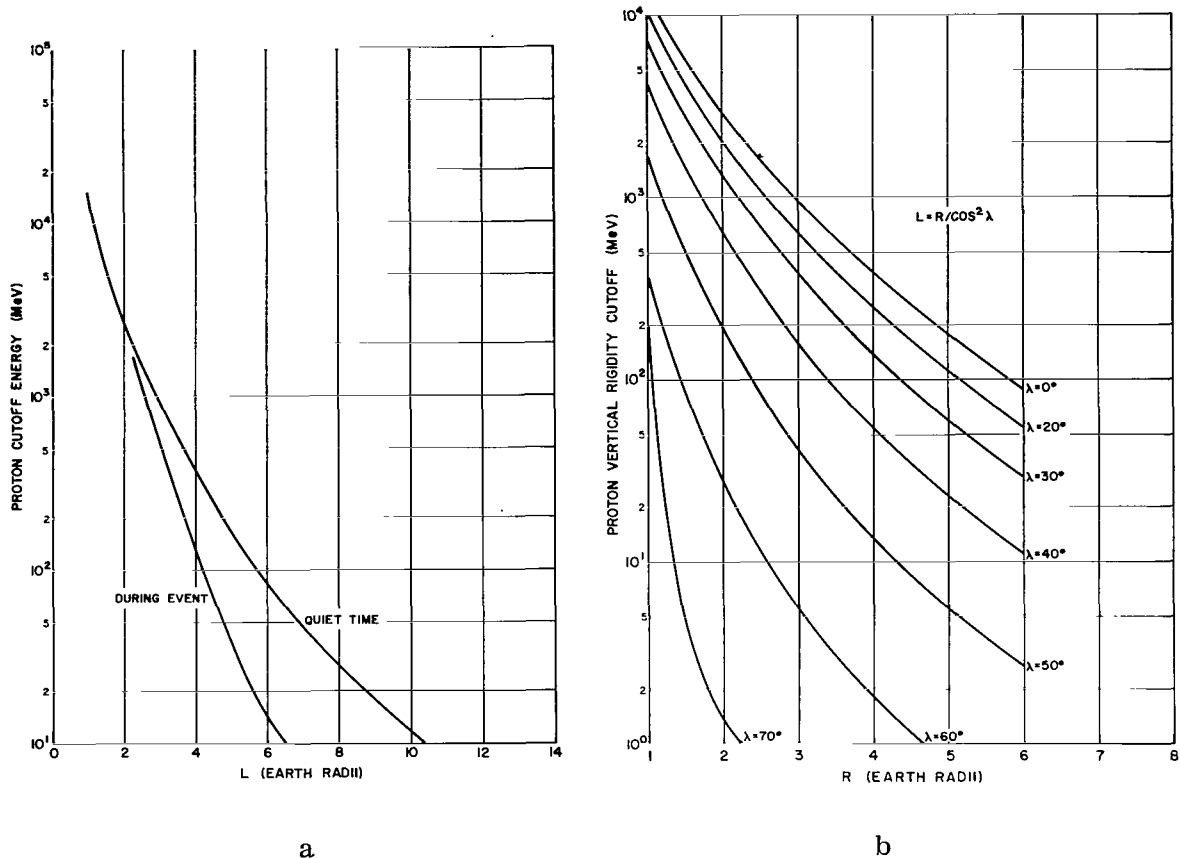
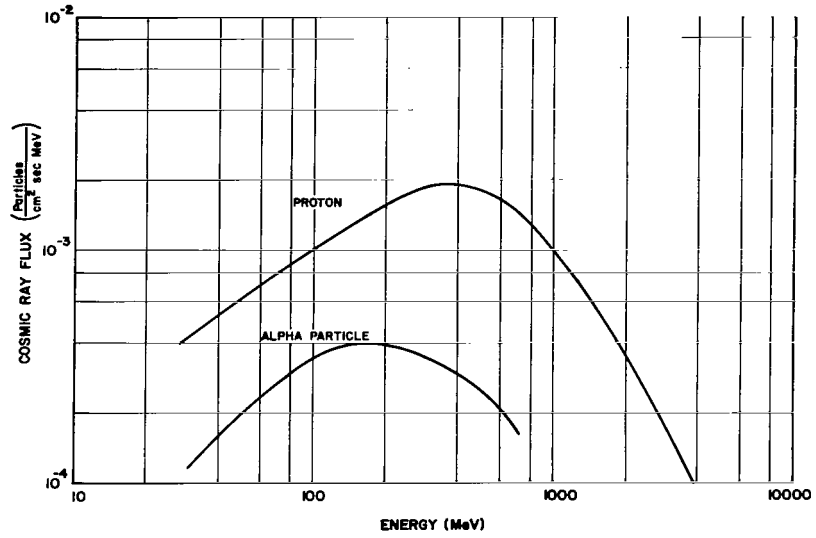


FIGURE 5. VARIATION OF PROTON VERTICAL CUTOFF ENERGY DURING A SOLAR ACTIVE PERIOD AND AS A FUNCTION OF EARTH RADII AND LATITUDE DURING QUIET TIME

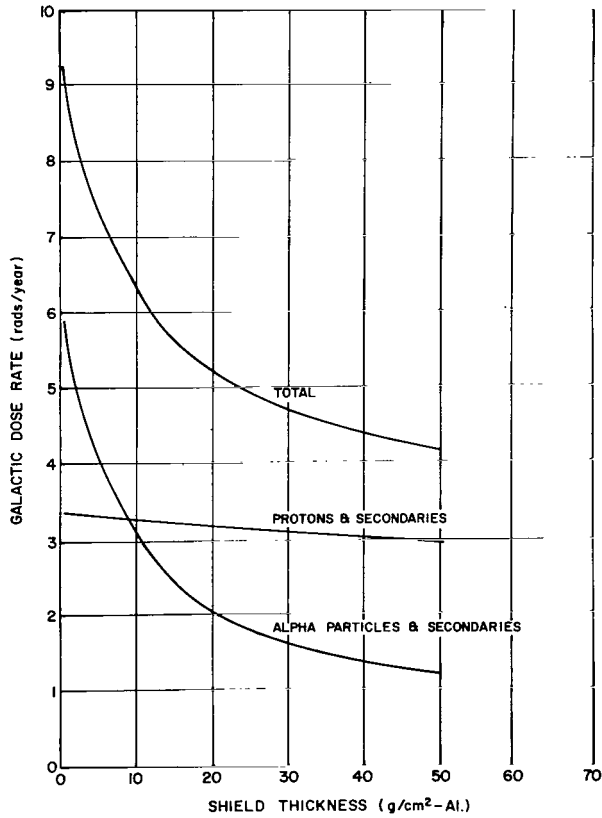
GALACTIC COSMIC RADIATION

The galactic cosmic radiation is composed of about 85 percent protons, 14 percent alpha particles, and about 1 percent heavier nuclei with energies ranging from 10^7 to 10^{19} eV, with an average energy of about 1 GeV. The free space proton flux at solar maximum is about 2.5 protons/cm²-sec and about twice this at solar minimum.

The differential energy spectrum [11] for protons and alpha particles is shown in Figure 6. The galactic cosmic ray dose rate (including secondaries) as a function of shield thickness is also shown in Figure 6. A spacecraft having an average thickness of 6 g/cm² of aluminum would receive a total dose of



a



b

FIGURE 6. GALACTIC COSMIC RAY DIFFERENTIAL ENERGY SPECTRA AND DOSE RATES BEHIND ALUMINUM SHIELDS

7.2 rads/year during solar minimum. At solar maximum the dose rate could be reduced by a factor of two. However, if one uses the modified energy spectrum as computed by the technique described on page 9, the total dose from cosmic radiation in a 30-degree, 240-nautical mile circular orbit would be on the order of 0.20 rad/year. Figure 7 shows the modified cosmic ray dose rate for protons plus secondaries as a function of orbital inclination on a 240-nautical mile circular orbit for an aluminum shield thickness of 10 g/cm². This graph does not include earth shadow effects.

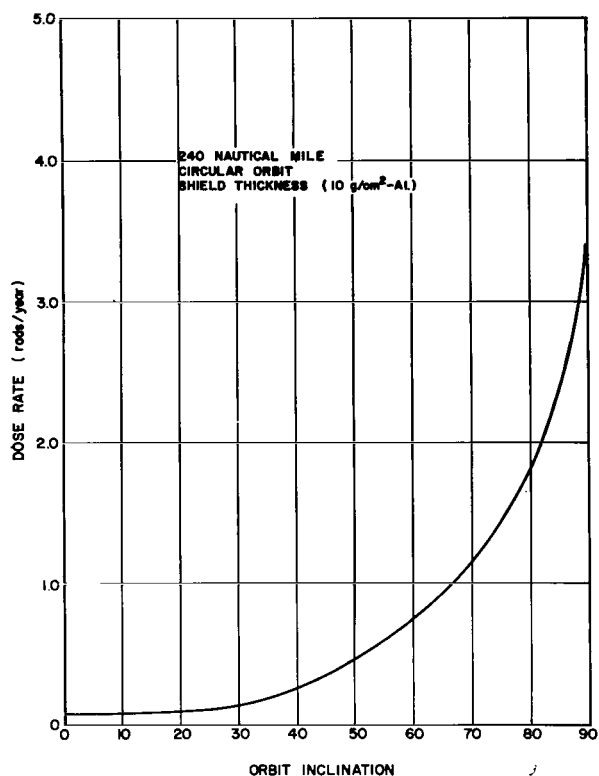


FIGURE 7. TOTAL COSMIC RAY PROTON DOSE RATE AS A FUNCTION OF ORBITAL INCLINATION

varying from 1 to 100. There is also a minor component of heavier nuclei which makes up about 0.1 percent of the total.

Results by some writers have implied that the dose rate is higher by a factor of two; however, insufficient data on their proton energy spectrum makes a comparison impossible.

SOLAR COSMIC RADIATION

The radiation intensity from solar flare activity follows an approximate 11-year cycle with enormous flux variations ranging from about 10⁵ protons/cm² at solar minimum to approximately 10⁹ protons/cm² per flare at solar maximum for protons with energy above 30 MeV. The solar radiation intensity will also vary with distance from the sun. The following solar proton data are assumed to be for a radial distance of one astronomical unit.

Solar cosmic radiation has two main components - protons and alpha particles in a proton-to-alpha ratio

The typical intensity-time profile for various rigidities in a solar cosmic ray event is shown in Figure 8. (Webber [12] provides detailed discussion.)

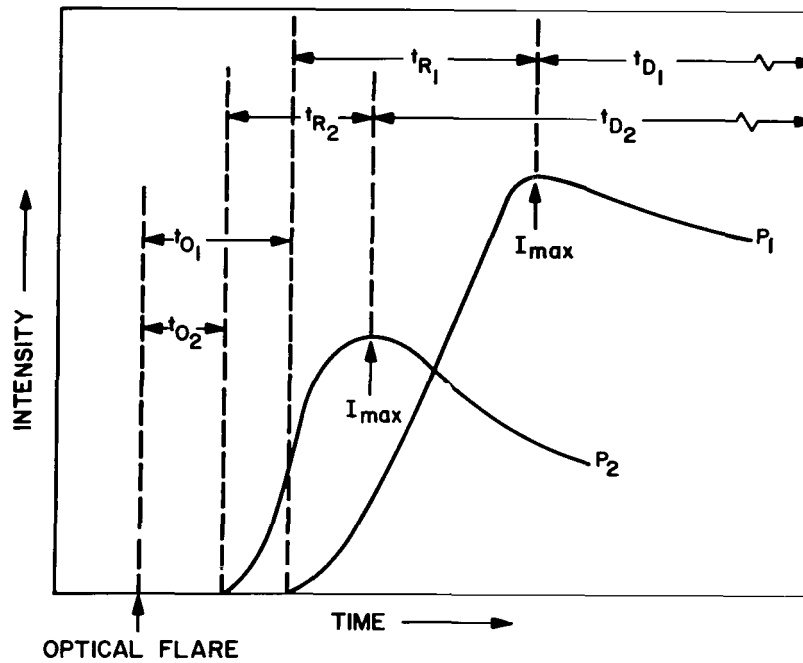


FIGURE 8. TYPICAL INTENSITY-TIME PROFILES DURING A SOLAR COSMIC RAY EVENT

The intensity follows an exponential increase to I_{\max} at $t = 0$ and an exponential decay beyond maximum intensity. The integrated intensity above a given energy is calculated using the characteristic rise and decay times given by

$$\begin{aligned}
J(>E) &= \int_{-\infty}^0 I_{\max}(>E) \exp\left(-\frac{t}{t_R}\right) dt + \int_0^{\infty} I_{\max}(>E) \exp\left(-\frac{t}{t_D}\right) dt \\
&= (t_R + t_D) I_{\max}(>E)
\end{aligned} \tag{5}$$

where I_{\max} is the maximum intensity at time $t = 0$; t_R = rise time; and t_D = decay time.

The time integrated spectrum describing the flux for a given event is given by

$$J(>p) = N_0 \exp\left(-\frac{p}{p_0}\right) \tag{6}$$

where p_0 (MV) is the characteristic rigidity, and N_0 is a constant determined from p_0 and $J(>p)$. Caution must be used in applying the same spectrum down to low rigidity values (<30 MeV).

To calculate the differential spectrum in MeV units using equation (6) [1], it is sufficient to use the relationship

$$p = \frac{1}{q} \sqrt{E^2 + 2ME} \tag{7}$$

and the Jacobian $\left| \frac{dp}{dE} \right|$ to obtain,

$$\phi(E) = \frac{N_0}{p_0} \exp\left(-\frac{p}{p_0}\right) \left| \frac{dp}{dE} \right| \frac{\text{particles}}{\text{cm}^2 - \text{MeV} - \text{Flare}}$$

or

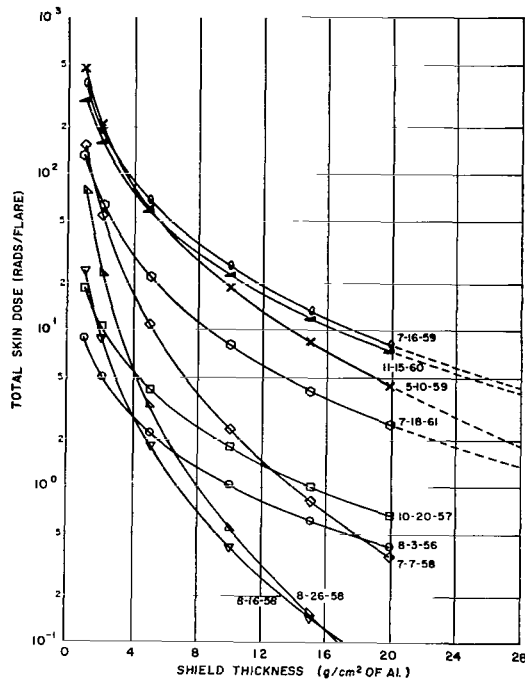
$$\phi(E) = \frac{N_0}{p_0 q} \left(\frac{E + M}{\sqrt{E^2 + 2ME}} \right) \exp\left(-\frac{\sqrt{E^2 + 2ME}}{p_0 q}\right) \frac{\text{particles}}{\text{cm}^2 - \text{MeV} - \text{Flare}}$$

where p is the rigidity (momentum/charge) in MV units, E is kinetic energy (MeV), q is the charge, and M is the rest mass energy (MeV). Thus, for protons, $q = 1$, and $M = 938$ MeV; for alpha rays, $q = 2$, and $M = 3727$ MeV.

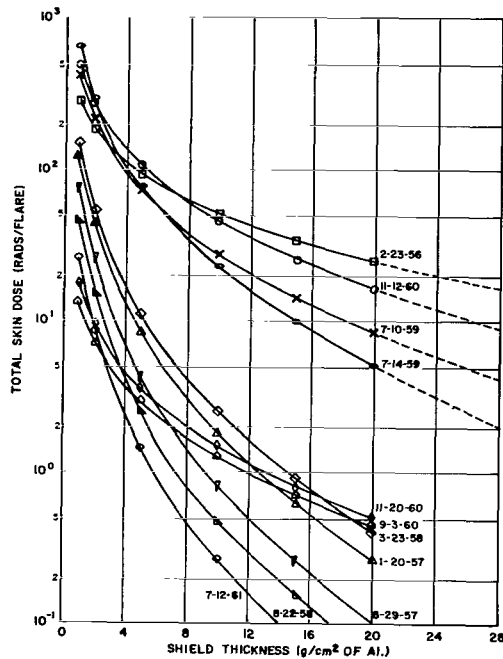
A list of the solar proton events [12] used in this study is shown in Table II. The solar proton events in Figure 9 represent the cases where the skin dose

TABLE II. INTEGRAL PROTON FLUX (PROTONS/cm²-FLARE) AT 30 AND 100 MeV WITH CORRESPONDING CHARACTERISTIC RIGIDITY P₀ AND N₀

Date	J(>30MeV)	J(>100MeV)	P ₀ (MV)	N ₀
2/23/56	1.0 × 10 ⁹	3.5 × 10 ⁸	195	3.41 × 10 ⁹
8/3/56	2.5 × 10 ⁷	6.0 × 10 ⁶	144	1.32 × 10 ⁸
1/20/57	2.0 × 10 ⁸	7.0 × 10 ⁶	61	1.02 × 10 ¹⁰
8/29/57	1.2 × 10 ⁸	3.0 × 10 ⁶	56	8.49 × 10 ⁹
10/20/57	5.0 × 10 ⁷	1.0 × 10 ⁷	127	3.30 × 10 ⁸
3/23/58	2.5 × 10 ⁸	1.0 × 10 ⁷	64	1.04 × 10 ¹⁰
7/7/58	2.5 × 10 ⁸	9.0 × 10 ⁶	62	1.18 × 10 ¹⁰
8/16/58	4.0 × 10 ⁷	1.6 × 10 ⁶	64	1.67 × 10 ⁹
8/22/58	7.0 × 10 ⁷	1.8 × 10 ⁶	56	5.02 × 10 ⁹
8/26/58	1.1 × 10 ⁸	2.0 × 10 ⁶	51	1.21 × 10 ¹⁰
9/22/58	6.0 × 10 ⁶	1.0 × 10 ⁵	50	7.21 × 10 ⁸
5/10/59	9.6 × 10 ⁸	8.5 × 10 ⁷	84	1.67 × 10 ¹⁰
7/10/59	1.0 × 10 ⁹	1.4 × 10 ⁸	104	1.00 × 10 ¹⁰
7/14/59	1.3 × 10 ⁹	1.0 × 10 ⁸	80	2.59 × 10 ¹⁰
7/16/59	9.1 × 10 ⁸	1.3 × 10 ⁸	105	8.92 × 10 ⁹
4/1/60	5.0 × 10 ⁶	8.5 × 10 ⁵	116	3.93 × 10 ⁷
4/28/60	5.0 × 10 ⁶	7.0 × 10 ⁵	104	5.01 × 10 ⁷
5/4/60	6.0 × 10 ⁶	1.2 × 10 ⁶	127	3.96 × 10 ⁷
5/13/60	4.0 × 10 ⁶	4.5 × 10 ⁵	94	5.09 × 10 ⁷
9/3/60	3.5 × 10 ⁷	7.0 × 10 ⁶	127	2.31 × 10 ⁸
9/26/60	2.0 × 10 ⁶	1.2 × 10 ⁵	73	5.29 × 10 ⁷
11/12/60	1.3 × 10 ⁹	2.5 × 10 ⁸	124	8.98 × 10 ⁹
11/15/60	7.2 × 10 ⁸	1.2 × 10 ⁸	114	5.89 × 10 ⁹
11/20/60	4.5 × 10 ⁷	8.0 × 10 ⁶	118	3.44 × 10 ⁸
7/11/61	3.0 × 10 ⁶	2.4 × 10 ⁵	81	5.77 × 10 ⁷
7/12/61	4.0 × 10 ⁷	1.0 × 10 ⁶	56	2.83 × 10 ⁹
7/18/61	3.0 × 10 ⁸	4.0 × 10 ⁷	102	3.13 × 10 ⁹
7/20/61	5.0 × 10 ⁶	9.0 × 10 ⁵	120	3.66 × 10 ⁷
9/28/61	6.0 × 10 ⁶	1.1 × 10 ⁶	121	4.33 × 10 ⁷
10/23/62	1.2 × 10 ⁵	1.0 × 10 ⁴	83	2.13 × 10 ⁷



a

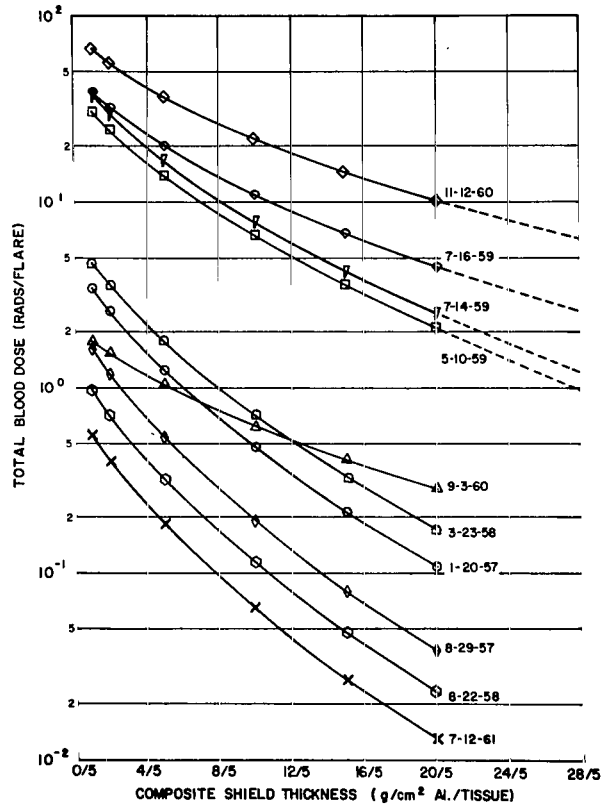


b

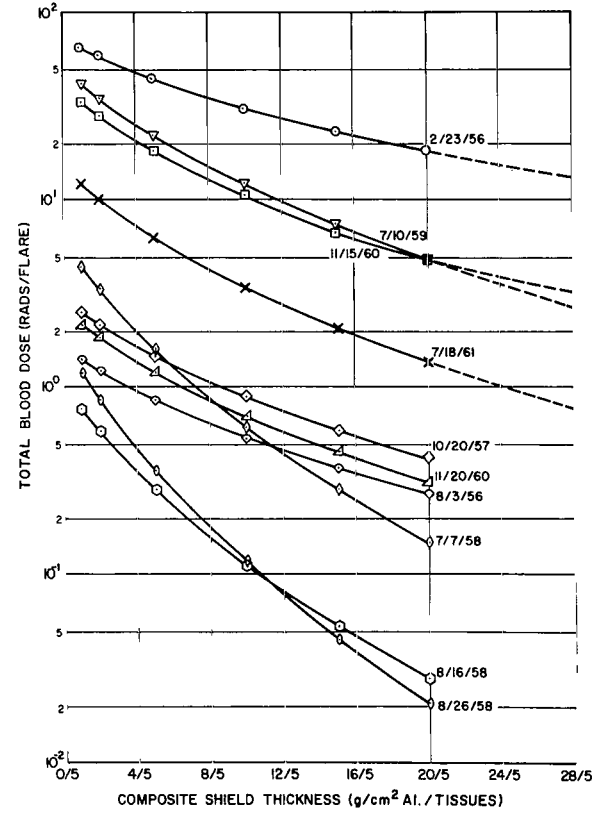
FIGURE 9. TOTAL PROTON SKIN DOSE BEHIND ALUMINUM SHIELDS FOR SEVERAL SOLAR FLARES

received behind 5 g/cm^2 aluminum shield is greater than about 1 rad. Figure 10 depicts solar cosmic ray doses at the blood-forming organs. Table III presents a summary from the above graphs. The proton skin dose behind polyethylene shields for the seven largest solar cosmic ray events is shown in Figure 11 and summarized in Table IV.

Figures 9 to 11 represent free space doses due to solar flare particles. Because of the geomagnetic field cutoff, the doses can be reduced by one or more orders of magnitude. Figure 12 depicts the modified energy spectra and corresponding dose rates for the November 12, 1960, flare on a 240-nautical mile circular orbit for various orbital inclinations. For an inclination of 45 degrees the dose is a constant of 0.0003 rad/flare. These dose values do not include earth shadow effects.



a



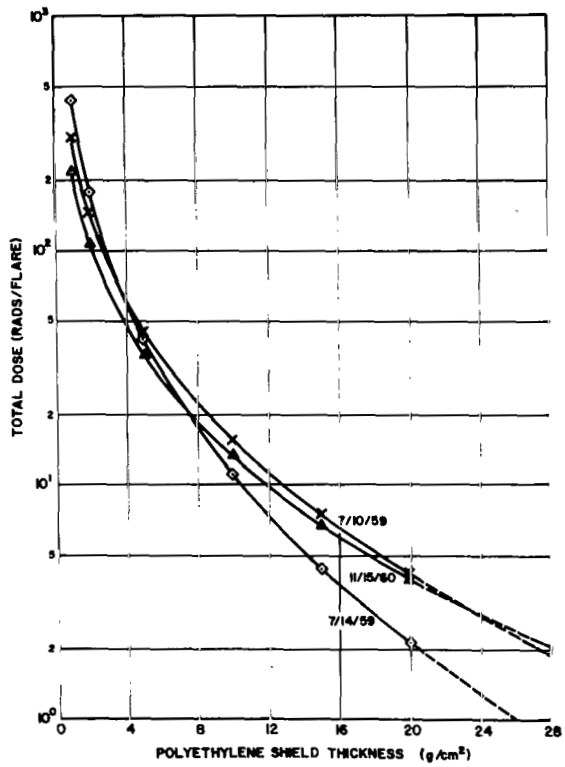
b

FIGURE 10. TOTAL PROTON BLOOD DOSE BEHIND ALUMINUM SHIELDS FOR VARIOUS SOLAR COSMIC RAY EVENTS

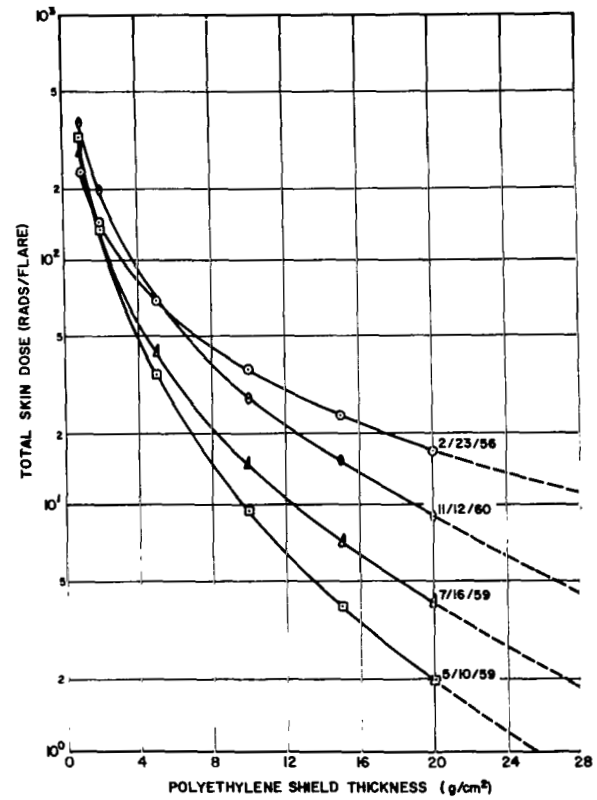
TABLE III. TOTAL ESTIMATED SOLAR FLARE DOSES BY EVENT
FOR TEN SHIELDING CONFIGURATIONS

Date	Shielding Configuration									
	1/0*	2/0	5/0	10/0	20/0	1/5	2/5	5/5	10/5	20/5
2/23/56	280.00	181.00	91.80	50.20	24.80	64.78	58.00	43.75	30.40	17.90
8/3/56	8.50	5.00	2.20	1.00	0.40	1.39	1.21	0.85	0.53	0.27
1/20/57	122.00	43.50	8.30	1.80	0.30	3.42	2.57	1.23	0.46	0.11
8/29/57	77.00	25.10	4.20	0.80	0.10	1.63	1.20	0.54	0.19	0.04
10/20/57	18.50	10.30	4.10	1.80	0.70	2.53	2.17	1.46	0.88	0.41
3/23/58	148.00	53.60	10.90	2.50	0.40	4.67	3.55	1.75	0.69	0.17
7/7/58	150.00	53.70	10.50	2.30	0.40	4.38	3.30	1.60	0.61	0.15
8/16/58	23.70	8.60	1.80	0.40	0.10	0.75	0.57	0.28	0.11	0.03
8/22/58	45.00	14.90	2.50	0.50	0.10	0.96	0.71	0.32	0.11	0.02
8/26/58	75.00	23.10	3.40	0.50	0.10	1.19	0.85	0.36	0.11	0.02
5/10/59	470.00	211.10	59.30	18.30	4.40	30.18	24.28	13.60	6.70	2.10
7/10/59	420.00	214.00	73.20	27.40	8.40	41.56	34.65	21.76	11.84	4.80
7/14/59	650.00	284.50	75.90	22.30	5.00	37.56	30.00	16.75	7.80	2.50
7/16/59	382.00	194.80	67.20	25.30	7.80	38.30	31.98	20.16	11.03	4.50
9/3/60	13.00	7.20	2.90	1.20	0.50	1.77	1.52	0.10	0.06	0.03
11/12/60	484.00	269.60	105.50	44.90	16.20	64.53	55.12	36.87	21.83	10.05
11/15/60	288.00	151.90	55.90	22.40	7.50	30.04	27.91	18.14	10.33	4.49
11/20/60	17.30	9.50	3.60	1.50	0.05	2.14	1.82	1.20	0.69	0.31
7/12/61	25.70	8.40	1.40	0.30	0.03	0.54	0.40	0.18	0.06	0.01
7/18/61	128.00	64.20	21.60	8.00	2.40	12.16	10.11	6.30	3.39	1.35

* Shielding configurations are given as X/Y where X = shielding thickness in g/cm² of aluminum and Y = shielding thickness in g/cm² of tissue.



a



b

FIGURE 11. TOTAL PROTON SKIN DOSE BEHIND POLYETHYLENE SHIELDS FOR SEVEN LARGE SOLAR COSMIC RAY EVENTS

TABLE IV. TOTAL ESTIMATED SOLAR FLARE DOSE
BEHIND POLYETHYLENE SHIELDS

Date	Shield Thickness					
	1*	2	5	10	15	20
2/23/56	226.8	141.5	68.4	35.7	23.1	16.5
5/10/59	317.8	134.1	33.6	9.3	3.8	1.9
7/10/59	303.0	145.7	45.5	15.5	7.5	4.2
7/14/59	435.0	177.5	42.1	11.0	4.4	2.1
7/16/59	275.2	133.0	41.9	14.4	7.0	4.0
11/12/60	366.1	192.4	69.8	27.5	14.7	9.0
11/15/60	210.0	106.0	35.9	13.3	6.8	4.0

* Shield thickness in g/cm^2 of polyethylene.

The November 12, 1960, proton spectral shape was somewhat controversial. The energy spectrum obtained by A. J. Masley [13] differs considerably from that of W. R. Webber (Table II) for energies below 100 MeV. Figure 13 is a comparison of skin doses using both Webber's and Masley's energy spectra.

The differential energy spectrum used by Masley is given by

$$J(E) = 1.77 \times 10^{13} E^{-3} \text{ cm}^{-2} \text{ MeV}^{-1} \quad (30 \leq E \leq 80 \text{ MeV})$$

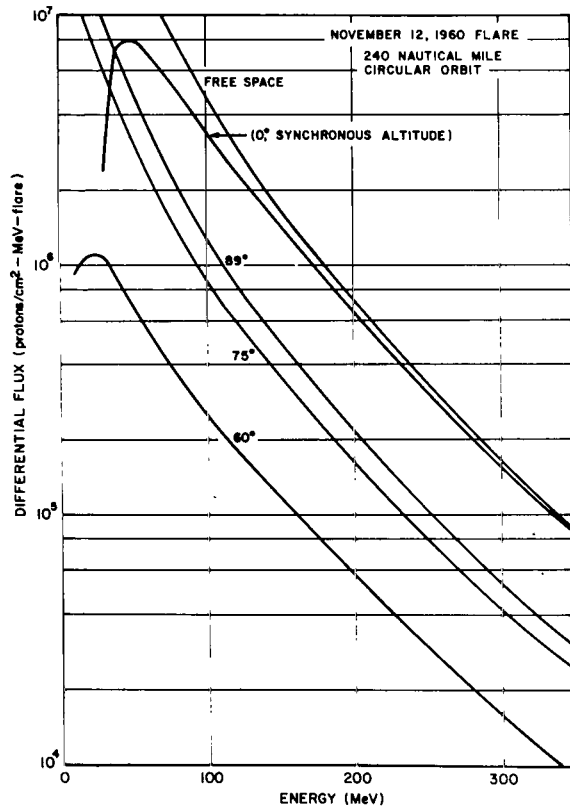
$$J(E) = 9.62 \times 10^{16} E^{-5} \text{ cm}^{-2} \text{ MeV}^{-1} \quad (80 \leq E \leq 440 \text{ MeV}) \quad (8)$$

$$J(E) = 6.63 \times 10^{18} E^{-5.4} \text{ cm}^{-2} \text{ MeV}^{-1} \quad (440 \leq E \leq 6600 \text{ MeV}).$$

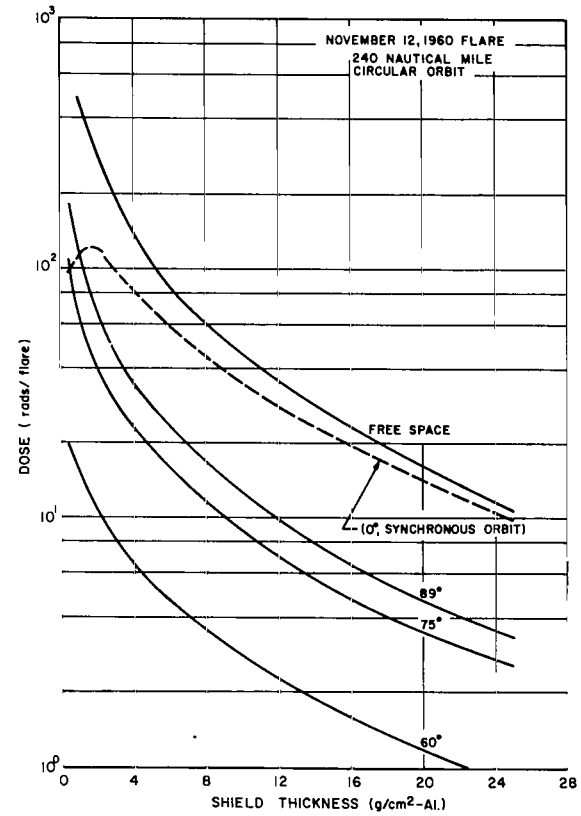
When comparing the results in the above figures, note that, using an aluminum shield of $6 \text{ g}/\text{cm}^2$, the dose at the blood-forming organs (5 cm of tissue) would be approximately the same for both spectra.

Figure 14 shows a parametric study of the dose received behind an aluminum shield for various values of the characteristic rigidity, p_0 . The proton integral spectrum in these calculations is given by

$$J(>p) = N_0 \exp\left(-\frac{p}{p_0}\right) = 10^9 \frac{\text{protons}}{\text{cm}^2} \quad (E > 30 \text{ MeV}) \quad (9)$$

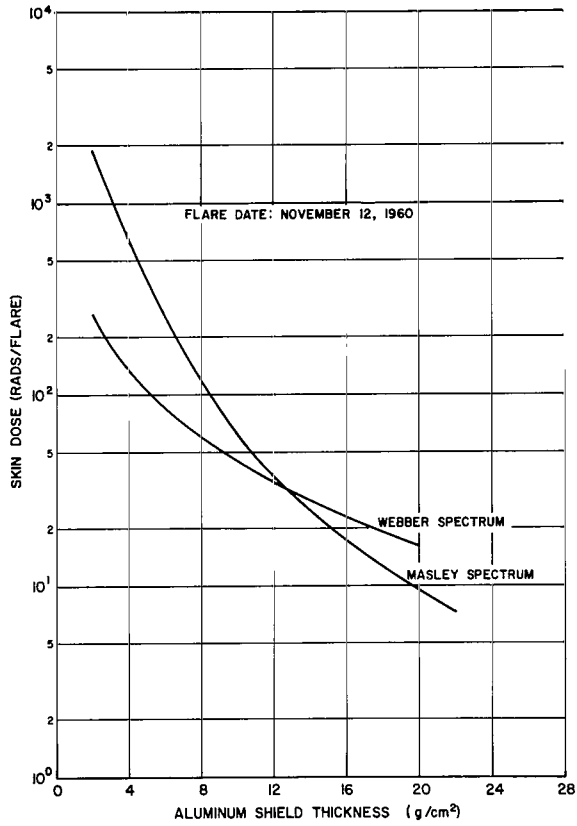


a

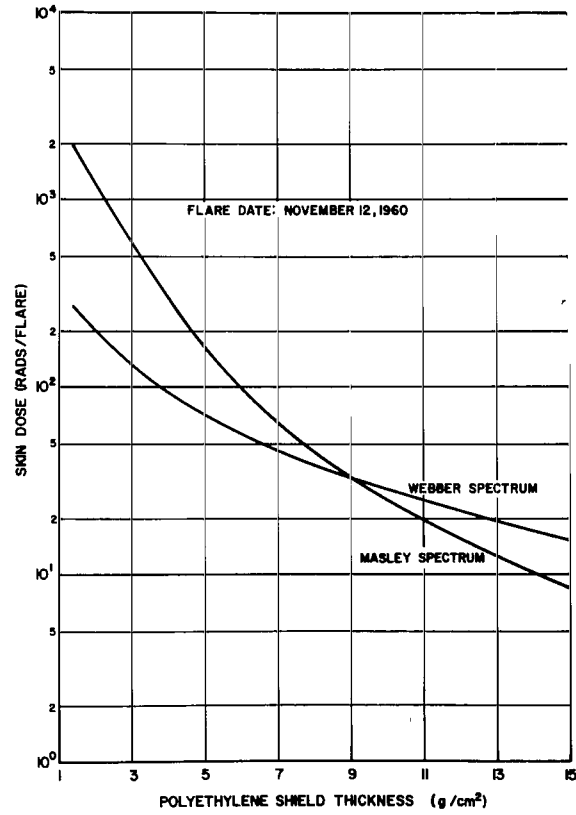


b

FIGURE 12. MODIFIED DIFFERENTIAL ENERGY SPECTRUM AND CORRESPONDING DOSE FOR THE NOVEMBER 12, 1960, SOLAR FLARE



a



b

FIGURE 13. COMPARISON OF TOTAL PROTON SKIN DOSE USING MASLEY AND WEBBER SPECTRA

and the characteristic rigidity, p_0 , is given for values between 50 and 200 MV.

Alpha particles seem to have about the same rigidity characteristics as protons. Figure 15 illustrates the characteristic rigidity plotted as a function of proton-to-alpha ratio [14].

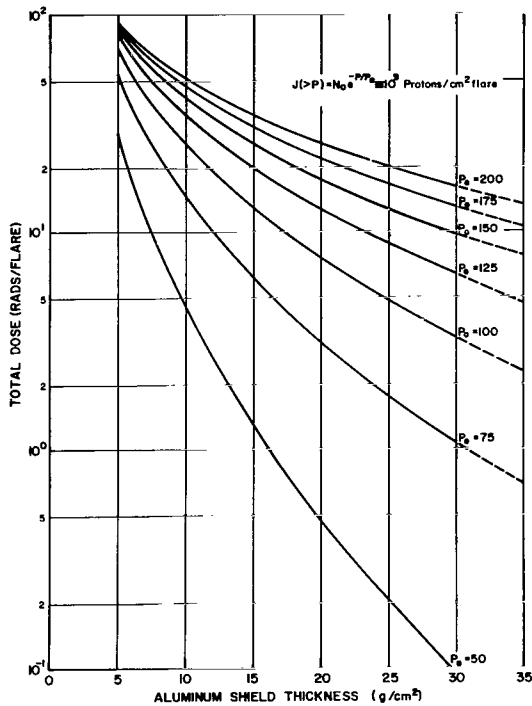


FIGURE 14. TOTAL PROTON SKIN DOSE BEHIND ALUMINUM SHIELDS FOR VARIOUS CHARACTERISTIC RIGIDITY VALUES

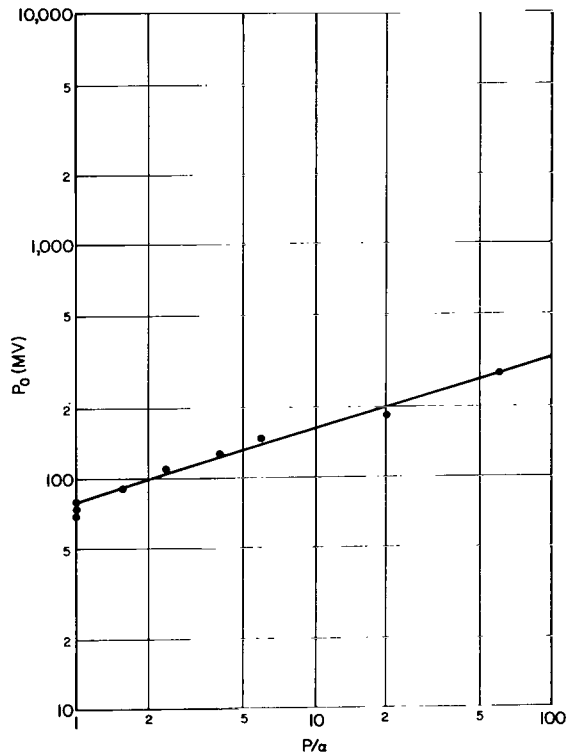


FIGURE 15. CHARACTERISTIC RIGIDITY AS A FUNCTION OF PROTON-TO-ALPHA RATIO

To evaluate the radiation dose derived from alpha rays, the large flare of July 10, 1959, was used. If alpha particles have the same rigidity as protons, the proton-to-alpha ratio for the above flare is about 2. The alpha rays' integral spectrum is given by

$$J(>p) = 5 \times 10^9 \exp\left(-\frac{p}{104}\right) \frac{\text{alphas}}{\text{cm}^2 - \text{Flare}} \quad (10)$$

The above alpha-ray energy spectrum was used for the comparison of the proton and alpha-ray skin dose as a function of aluminum shield thickness in Figure 16. For an aluminum shield thickness of 4 g/cm², the proton dose is a factor of 10 above the alpha dose.

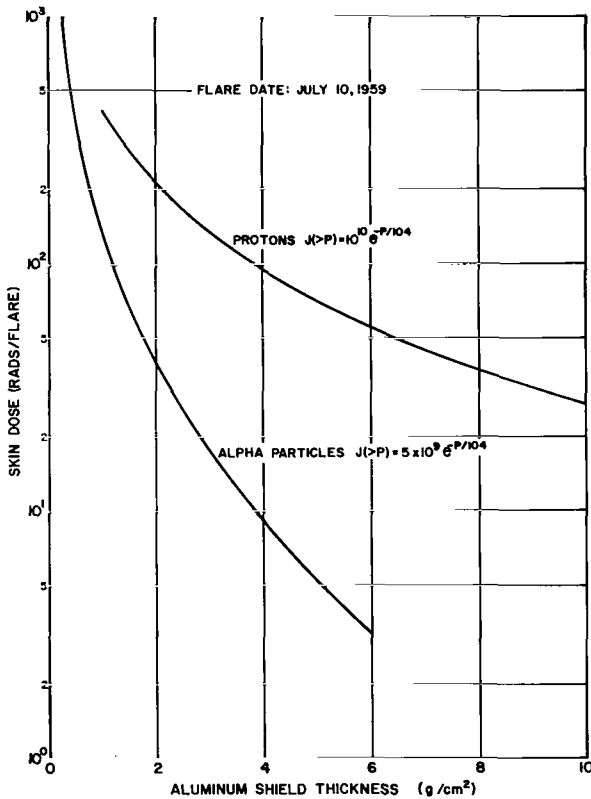


FIGURE 16. A COMPARISON OF PROTON AND ALPHA RAY SKIN DOSE AS A FUNCTION OF ALUMINUM SHIELD THICKNESS

PREDICTION OF SOLAR PROTON EVENTS

Because of the importance of solar protons in the manned space flight program, it seems justifiable to discuss the methods and status of flare predictions. Many statistical studies have been undertaken, but not too much reliance can be placed on these studies since the sample of data is rather small. It should be pointed out that each flare differs from all others so that no exact relationship exists between observable features. A proper statistical analysis must involve a large number of events to permit specific statements about flare occurrence, duration, and intensity.

Because of the rotation of the sun there exists an east-west asymmetry of solar proton events. For events occurring on the Eastern Hemisphere of the sun, the probability of solar protons reaching the earth is one-third that of events occurring on the

the Western Hemisphere [12]. If an event does occur on the Eastern Hemisphere the corresponding onset, rise, and decay times are three times greater than that of events on the western half, giving astronauts more time to prepare for the oncoming event.

The presence and development of an active region with its associated sunspots and complex magnetic field is a basic part of the process which leads to a solar cosmic ray event. Thus, it is found that there are two aspects of primary importance for flare prediction [15] and warning capabilities. These are (1) the persistence of single active centers, and (2) the magnetic configurations of these active centers. Regarding the persistence of single active centers, Guss [16] has pointed out that a single fixed location in solar longitude produced most of the major events in cycle 19. During a period of over five years (more than 73 rotations), several active centers grew and died in this same local region on the sun. These major events included the events of February 23, 1956, July 1959, November 1960, and July 1961. About 75 percent of the total integrated particle intensity above 10 MeV came from this one "hot" location. According to Webber [12], over 90 percent of the output of the solar cosmic rays above 10 MeV came from only eight major active centers during solar cycle 19. Four of these were associated with this one particular location. If a "hot" region exists and can be identified early in a solar cycle, the prediction of large events will probably be concerned with the study of this one region.

According to Weddell [17], there seems to be a linear correlation between the smoothed sunspot number and the number of cosmic ray events, and also with the integrated intensity of particles above 10 MeV. The number of annual particle events [12] occurring at the next solar maximum should be about four or five, with an annual integrated intensity above 10 MeV of about 10^9 particles/cm² based on results of solar cycle 19. According to Webber [18] the maximum sunspot number should occur near the middle of 1968 and could have a value of 110-130.

The distribution of the integrated flux per event [17] as a function of the number of events for cycle 19 is given in Figure 17. The monthly probabilities of events as a function of event size over the 96-month period from 1956 through 1963 for 68 flare events is shown in Figure 18.

Tabulated data showed that during the solar cycles from 1942 through 1963 (covering 76 observed events [17]), July was by far the most active month, with 18.4 percent; September was the second most active, with 17.1 percent; August was the third most active with 13.2 percent, and December, with no observed events, has apparently been the least active month.

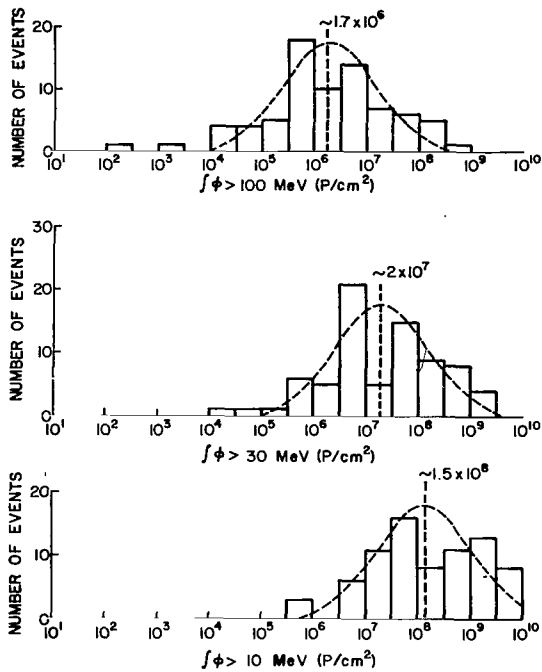


FIGURE 17. DISTRIBUTION OF THE INTEGRATED FLUX PER EVENT AS A FUNCTION OF THE NUMBER OF EVENTS FOR SOLAR CYCLE 19

Dr. J. E. Norman of the University of Georgia [19] in conjunction with M. O. Burrell and J. W. Watts developed a stochastic model for the prediction of expected proton doses on space missions beyond the earth's magnetosphere. In this study, the model was based on the available solar flare data from cycle 19, the last complete cycle. Point skin doses inside spherical shells of aluminum of 2, 5, 10, and 20 g/cm² thicknesses were calculated for each of the important solar flares observed during the 312 weeks of the active period. An important flare was considered to be one which gave one rad of dose behind a 2 g/cm² shield. Using this data, the authors developed a Monte Carlo model based on four assumptions. These assumptions were:

1. The size and number of flares in any future active period were based on the distribution of the 19th cycle flares.

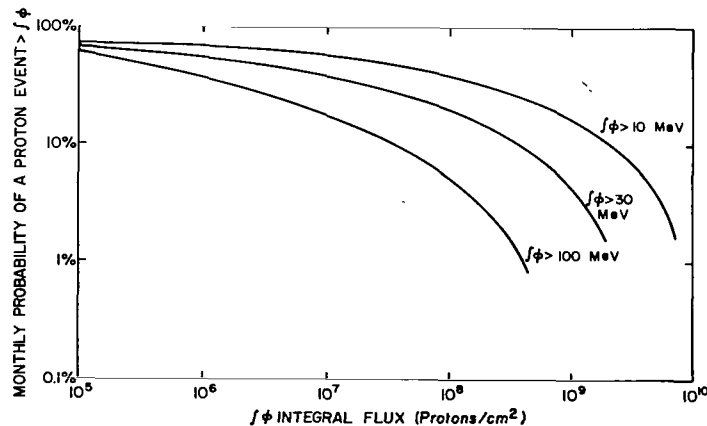


FIGURE 18. MONTHLY PROBABILITY OF A PROTON EVENT AS A FUNCTION OF EVENT SIZE

2. An event was assumed to consist of one, two, or three flares in the period of a week in the same ratios observed in the 19th cycle. There were 31 flares in the 19th cycle making up 25 weekly events consisting of 20 single flares, 4 double flares, and 1 triple flare.
3. Flares making up an event were of the same size.
4. The events were distributed randomly in time over the 6-year active period.

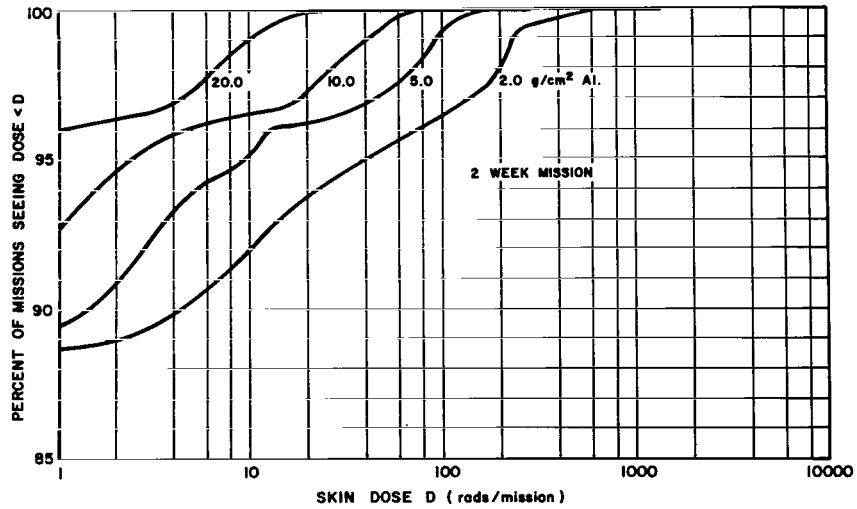
The individual weeks of a mission were generated by random sampling based on these assumptions. Twenty thousand missions were generated, and a cumulative probability distribution was formed. Figure 19 shows these distributions for missions of 2 and 52 weeks for the four shielding thicknesses. Figure 20 shows dose vs shield thickness for the given cumulative probabilities. For example, in Figure 20 the 95 percent curve means that 95 percent of the missions had doses below those shown.

TRAPPED PROTONS

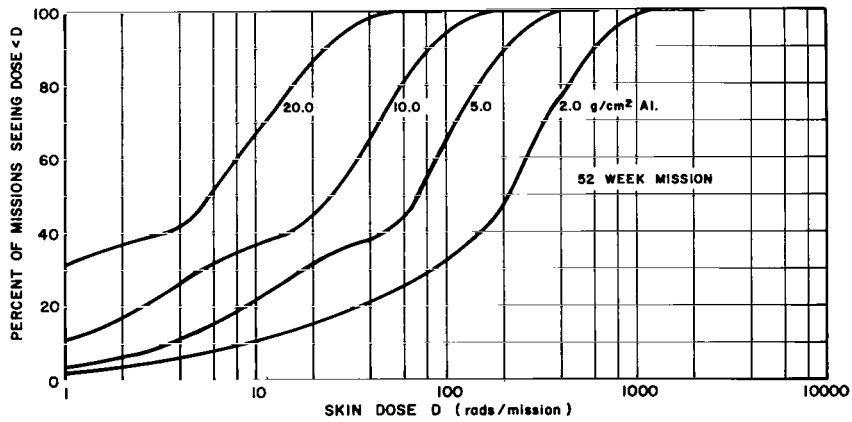
The proton environmental data used in this study were taken from the work of James I. Vette [20] of Goddard. The proton flux above four different threshold energies is shown in Figures 21 and 22. These fluxes are for circular orbits at different altitudes above the earth for 0-, 30-, 60- and 90-degree orbital inclinations respectively. The skin dose rates calculated from the AP3 spectral data are shown in Figures 23 through 26. The AP3 data were extended down to 40 MeV to obtain the proton dose rates for the 2 g/cm^2 cases.

The above proton dose calculations include primary and secondary particles, and the dose is computed for a point at the center of a spherical shell of indicated shield thickness. No self-shielding by astronauts is included; hence, doses are high by approximately a factor of two for human targets.

Figure 27 shows an isoflux plot in the south Atlantic anomaly at an altitude of 400 kilometers. Figure 28 depicts the integral flux received on a 30-degree circular orbit at an altitude of 240 nautical miles as a function of time.

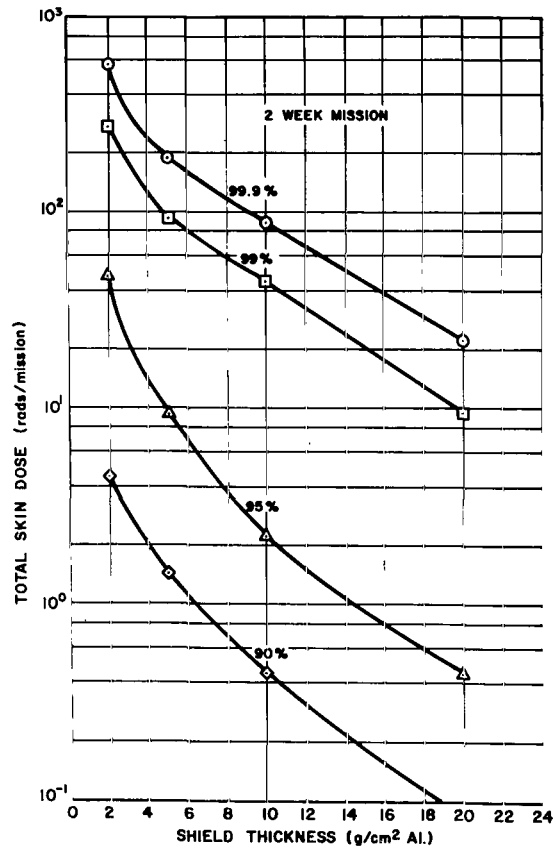


a

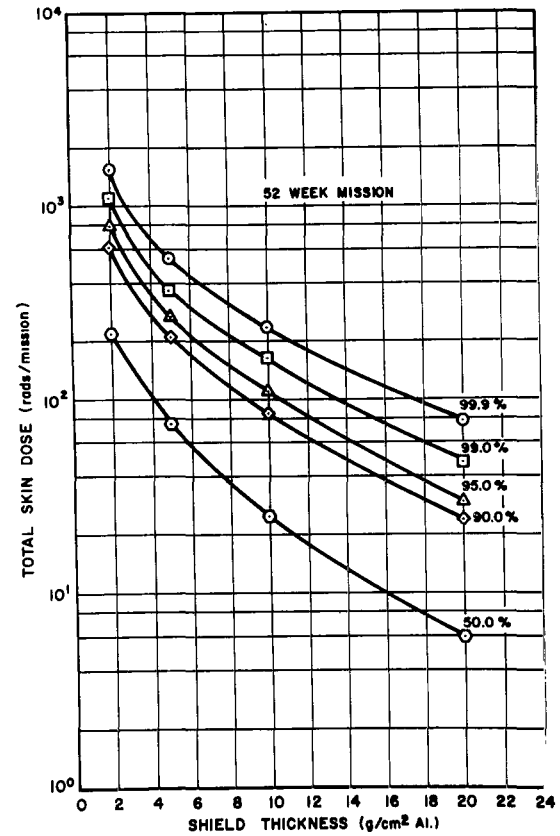


b

FIGURE 19. CUMULATIVE PROBABILITY DISTRIBUTIONS FOR 2 AND 52 WEEK MISSIONS AS A FUNCTION OF DOSE FOR VARIOUS SHIELD THICKNESSES

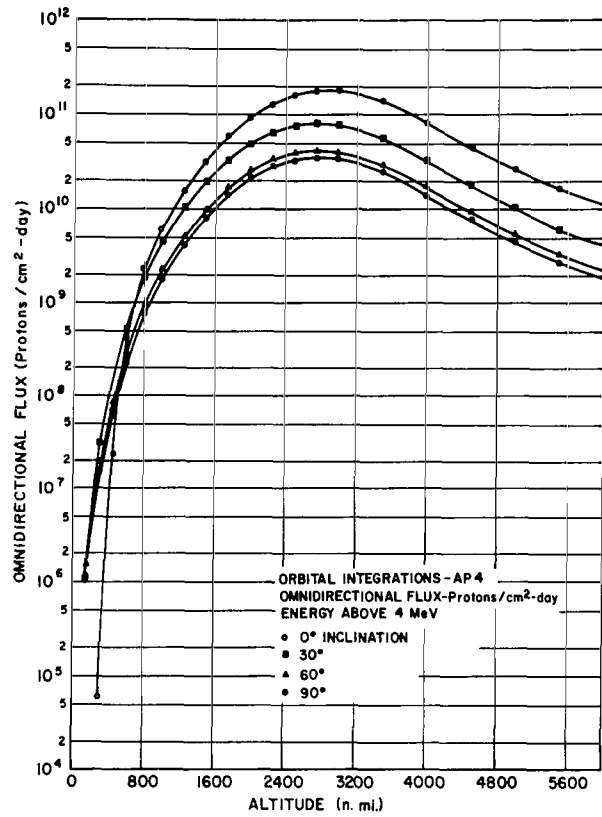


a

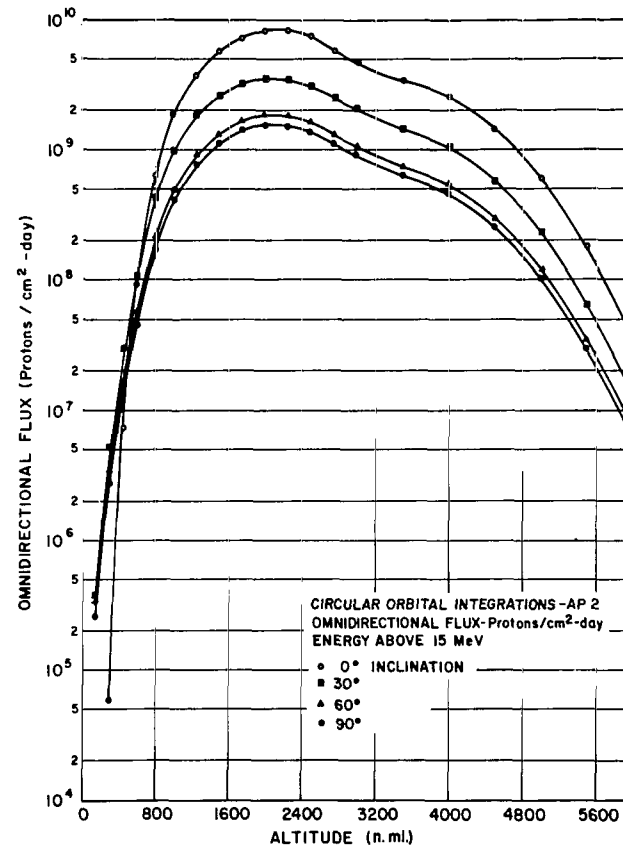


b

FIGURE 20. DOSES RECEIVED ON 2 AND 52 WEEK MISSIONS AS A FUNCTION OF SHIELD THICKNESS FOR VARIOUS CUMULATIVE PROBABILITIES

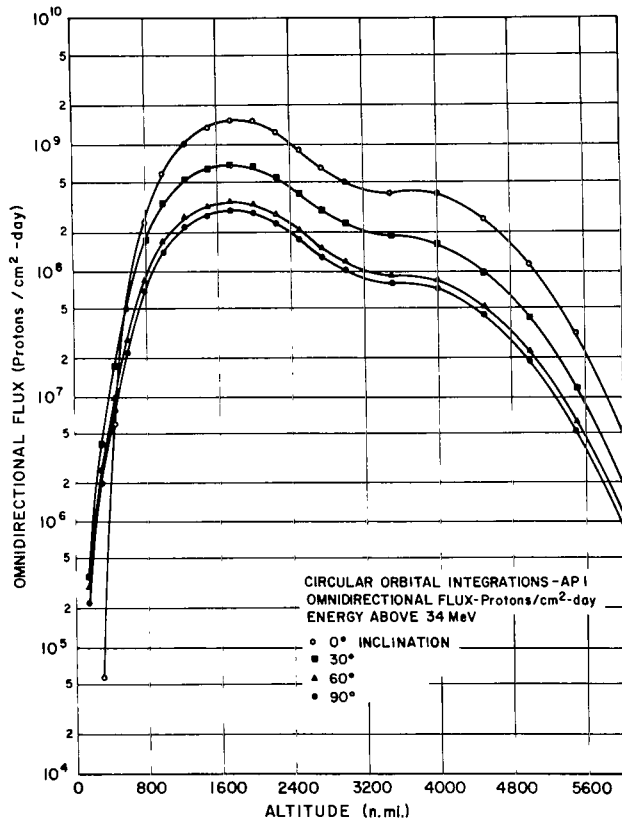


a

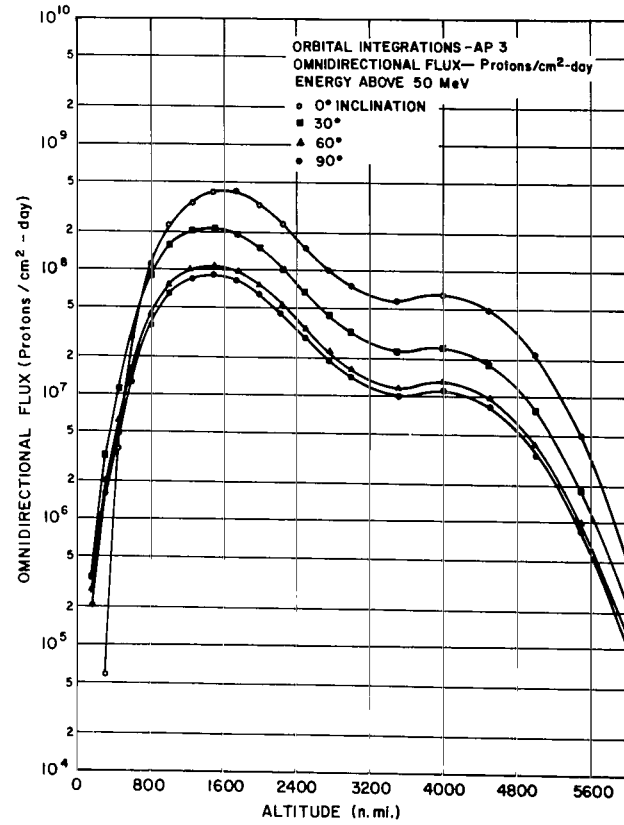


b

FIGURE 21. TRAPPED OMNIDIRECTIONAL PROTON FLUX ABOVE 4 AND ABOVE 15 MeV

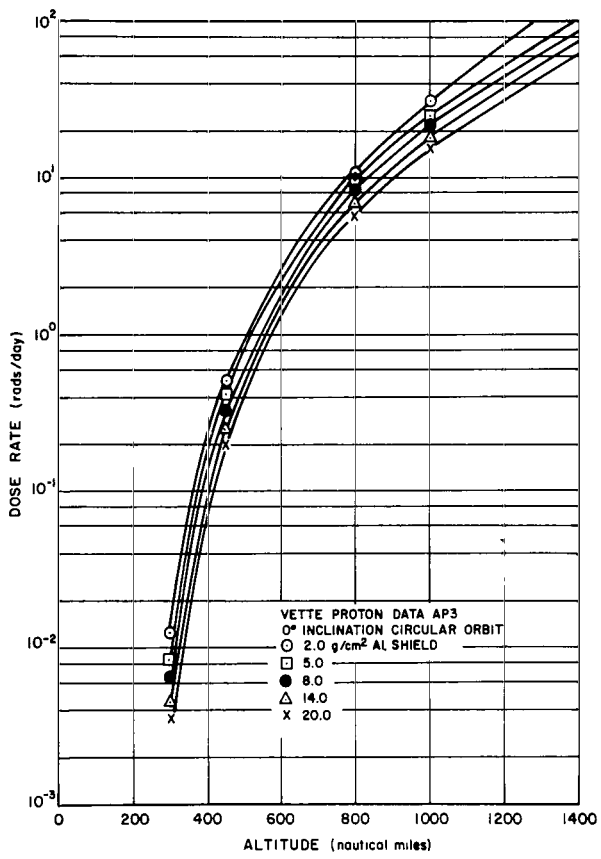


a

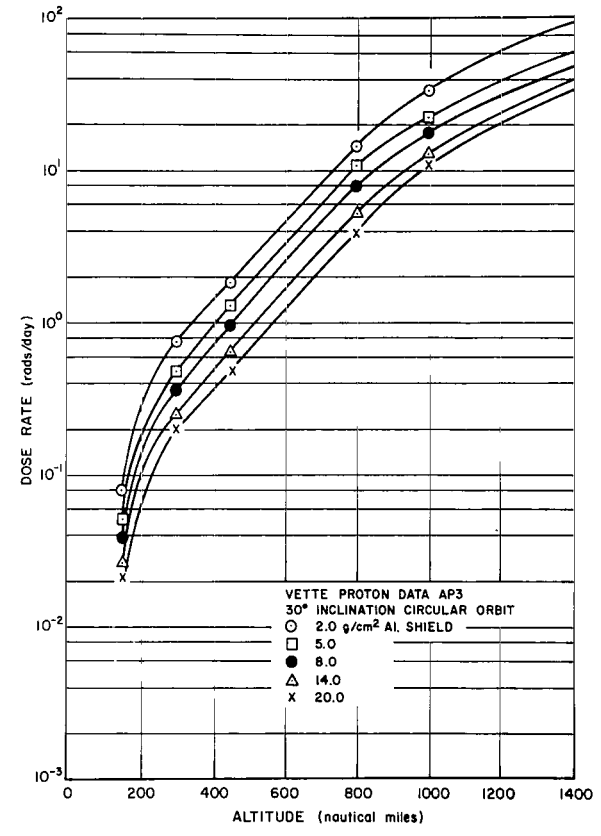


b

FIGURE 22. TRAPPED OMNIDIRECTIONAL PROTON FLUX ABOVE 34 AND ABOVE 50 MeV

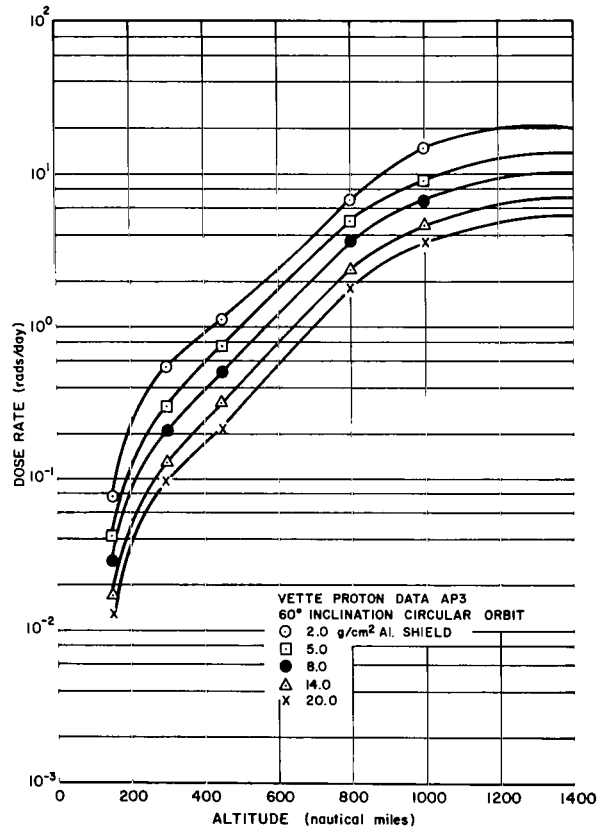


a

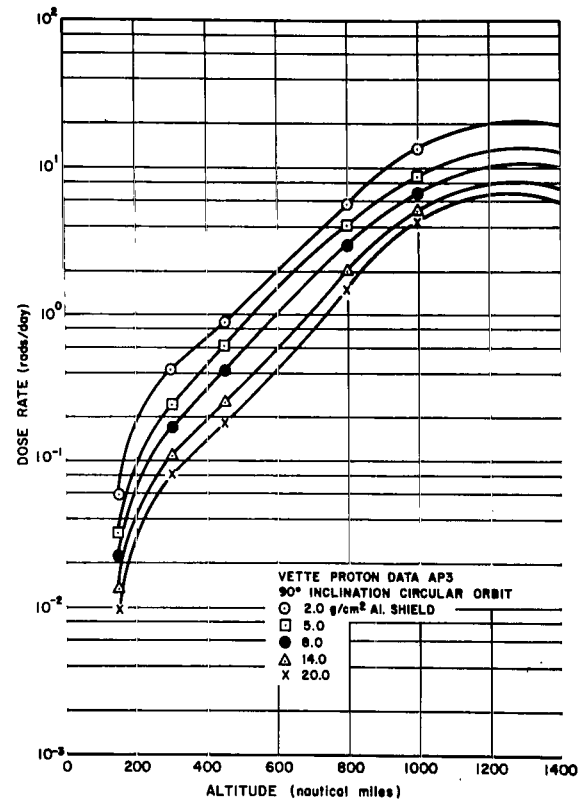


b

FIGURE 23. LOW ALTITUDE TOTAL PROTON DOSE RATE AS A FUNCTION OF SHIELD THICKNESS AND ALTITUDE FOR 0- AND 30-DEGREE ORBITAL INCLINATIONS

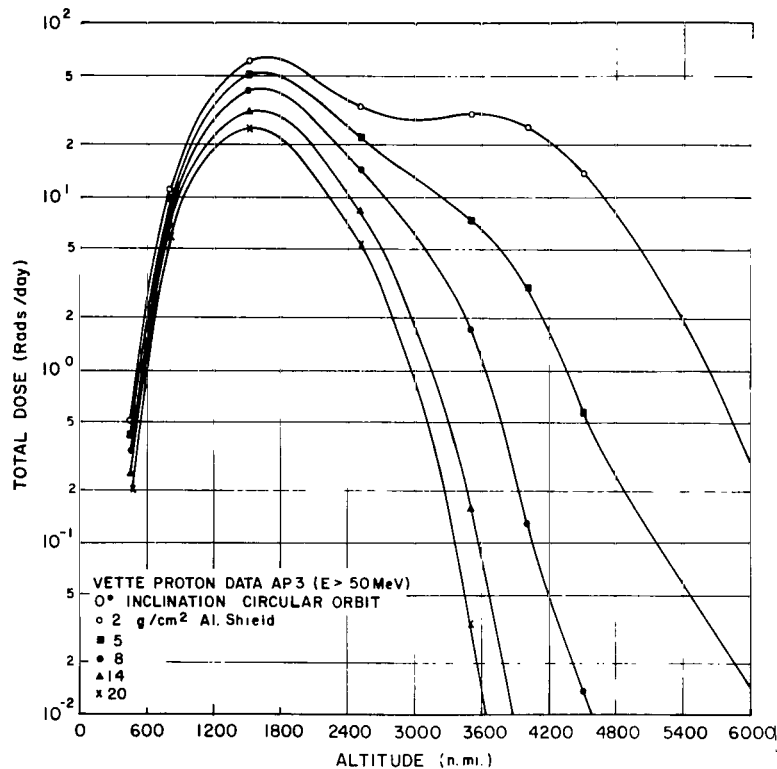


a

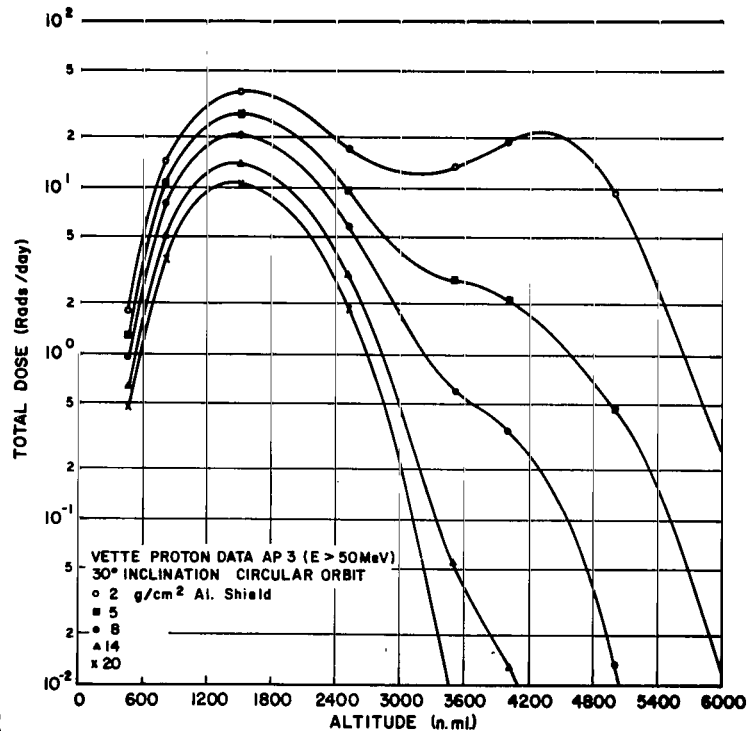


b

FIGURE 24. LOW ALTITUDE TOTAL PROTON DOSE RATE AS A FUNCTION OF SHIELD THICKNESS AND ALTITUDE FOR 60- AND 90-DEGREE ORBITAL INCLINATIONS

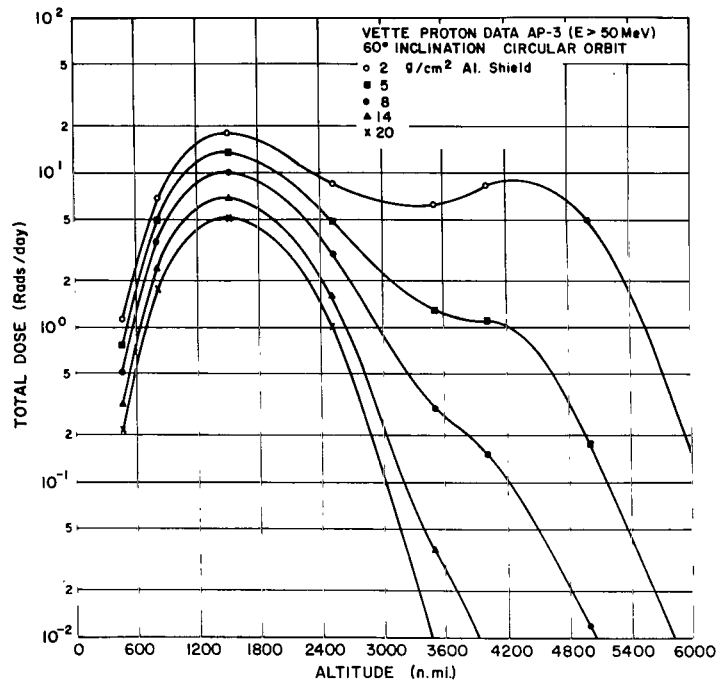


a

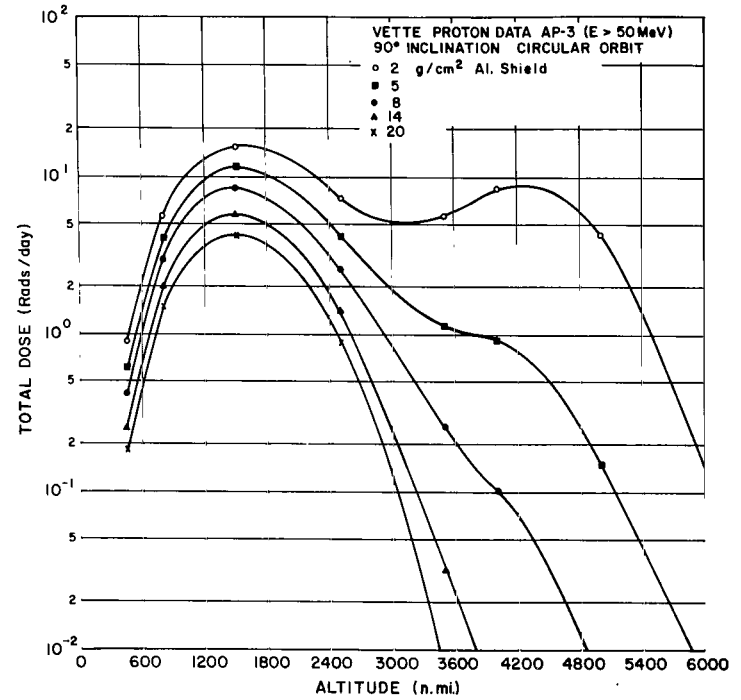


b

FIGURE 25. TOTAL PROTON DOSE RATE AS A FUNCTION OF SHIELD THICKNESS AND ALTITUDE FOR 0- AND 30-DEGREE ORBITAL INCLINATIONS



a



b

FIGURE 26. TOTAL PROTON DOSE RATE AS A FUNCTION OF SHIELD THICKNESS AND ALTITUDE FOR 60- AND 90-DEGREE ORBITAL INCLINATIONS

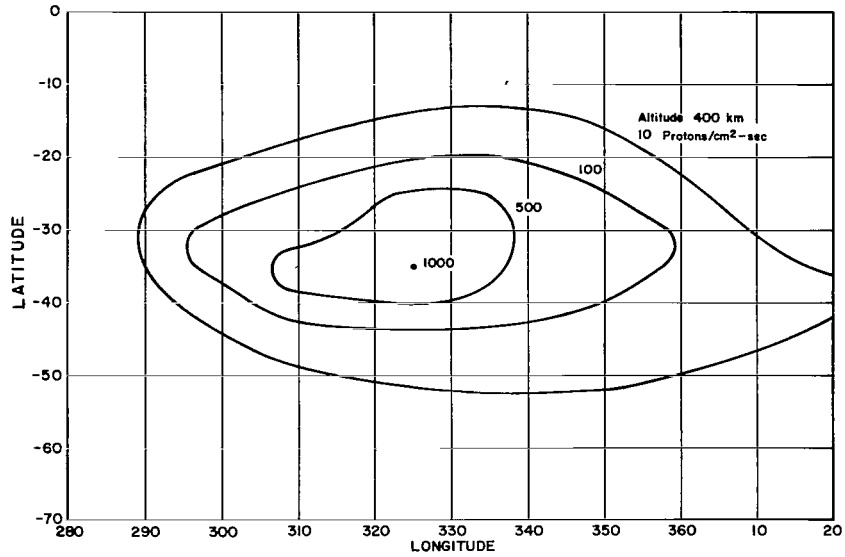


FIGURE 27. PROTON ISOFLUX PLOT AT AN ALTITUDE OF 400 km IN THE SOUTH ATLANTIC ANOMALY

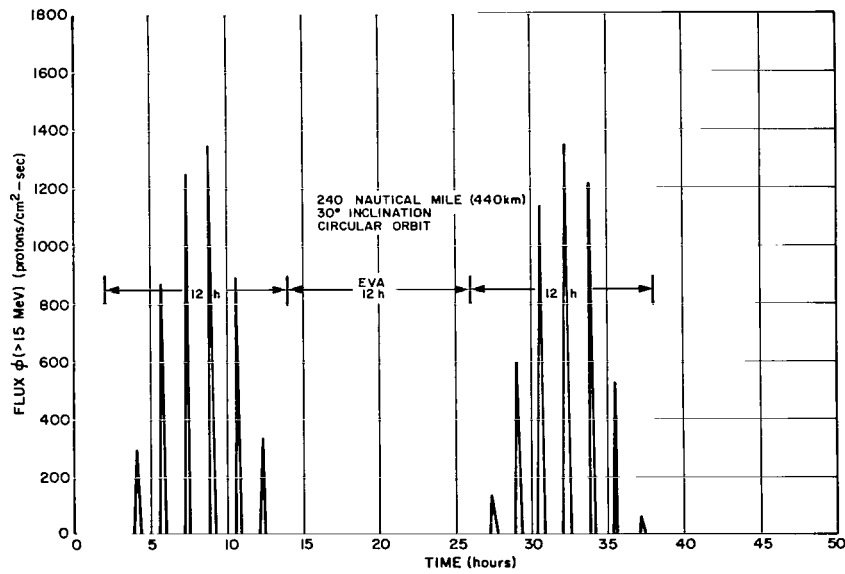


FIGURE 28. INTEGRAL PROTON FLUX RECEIVED ON A 30-DEGREE CIRCULAR ORBIT AT AN ALTITUDE OF 240 NAUTICAL MILES

TRAPPED ELECTRON AND BREMSSTRAHLUNG RADIATION

Dr. Vette [21] has produced a projected electron environment for December 1968 starting with the August 1964 AE2 electron environment. He decreased the number of electrons in the inner belt according to the measurements of Bostron, et al. [22], and increased the number of electrons in the outer belt to correspond to solar maximum conditions. Figure 29 shows the 1968 data as compared to the 1964 electron data. Figures 30 to 33 show the electron and corresponding bremsstrahlung dose rates for the 1968 electron environment. (Bremsstrahlung is the electromagnetic radiation produced by the acceleration and deceleration of electrons in nuclear electric fields.)

The 1964 electron environmental data and the related electron and bremsstrahlung dose rates have been placed in the appendix. The 1968 data are now considered to be the best available environmental model for planning purposes. The development of a new electron environmental model is being pursued by Dr. Vette at Goddard, but may not be forthcoming until the effects of the present solar cycle are better known.

A typical bremsstrahlung dose transmission curve is shown in Figure 34 for isotropically incident electrons with an energy spectrum given by

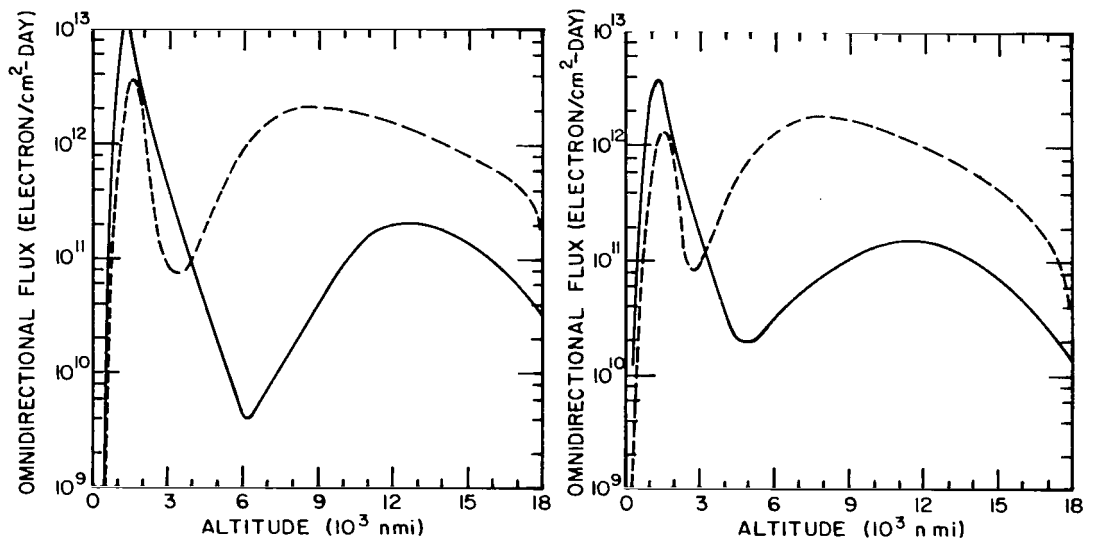
$$\phi(>E) = 10^{13} \exp(-2E) \frac{\text{electrons}}{\text{cm}^2 - \text{day}} \quad (11)$$

The bremsstrahlung dose is not strongly dependent on aluminum thickness, as shown in Figure 34. However, the bremsstrahlung is primarily of low energy and its intensity can be greatly reduced by adding a thin layer of lead on the inside of the shield. For shields thicker than about 2 g/cm² the bremsstrahlung dose is the most important radiation hazard associated with electrons. The isotropic incidence assumption is more valid for electrons and associated bremsstrahlung dose calculations than a simple straight ahead approximation.

The electron and bremsstrahlung dose rates as a function of shield thickness are shown in Figure 35 for a model electron integral spectrum given by

$$\phi(>E) = N_0 \exp\left(-\frac{E}{E_0}\right) \quad (12)$$

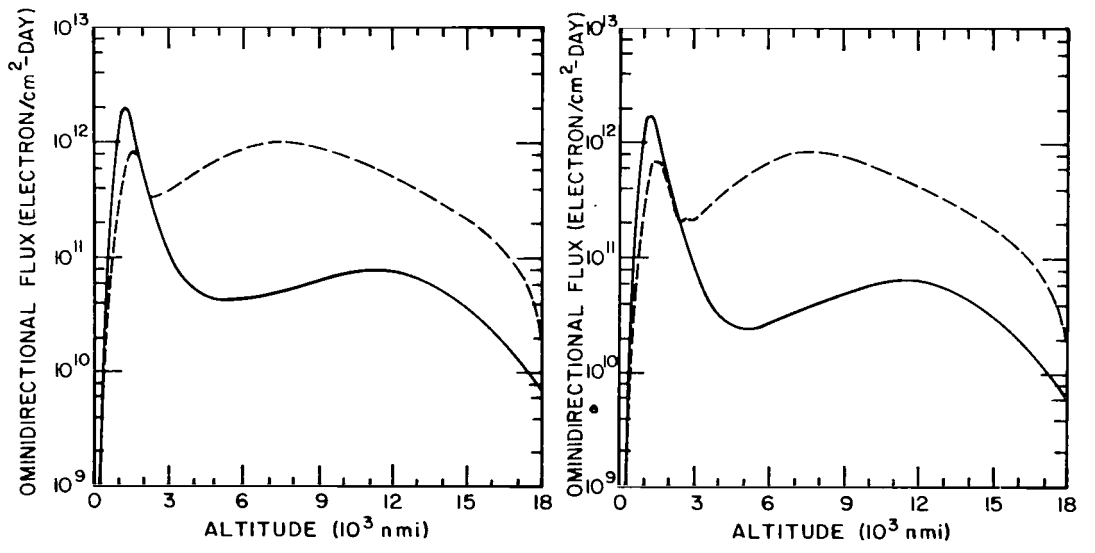
with $\phi(>0.5) = 10^{10}$ electrons/cm² - day and the values of E_0 are chosen between 0.25 and 1.25 MeV.



COMPARISON OF ORBITAL INTEGRATIONS AT 0° INCLINATION.

COMPARISON OF ORBITAL INTEGRATIONS AT 30° INCLINATION.

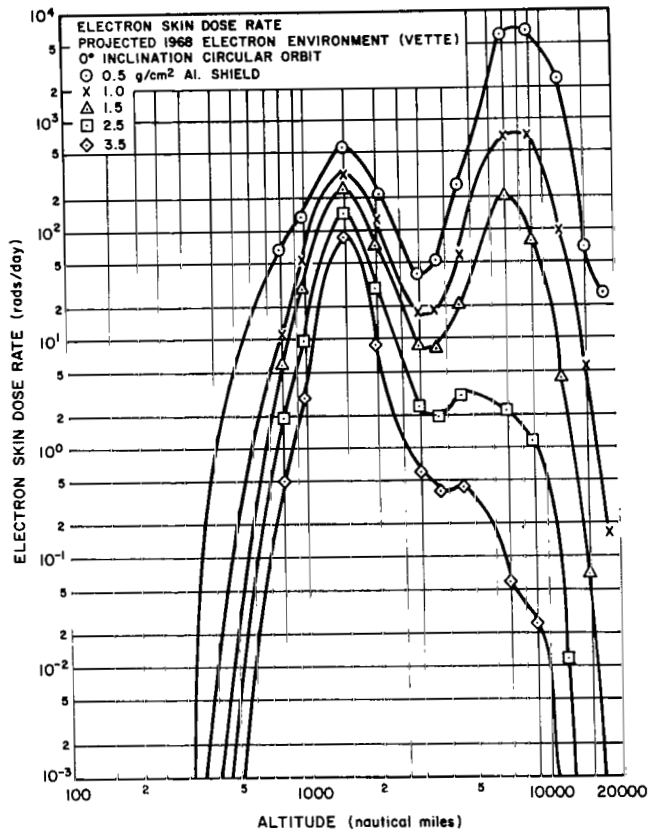
AE2 MAP AUGUST 1964
 PROJECTED 1968 MAP DECEMBER 1968



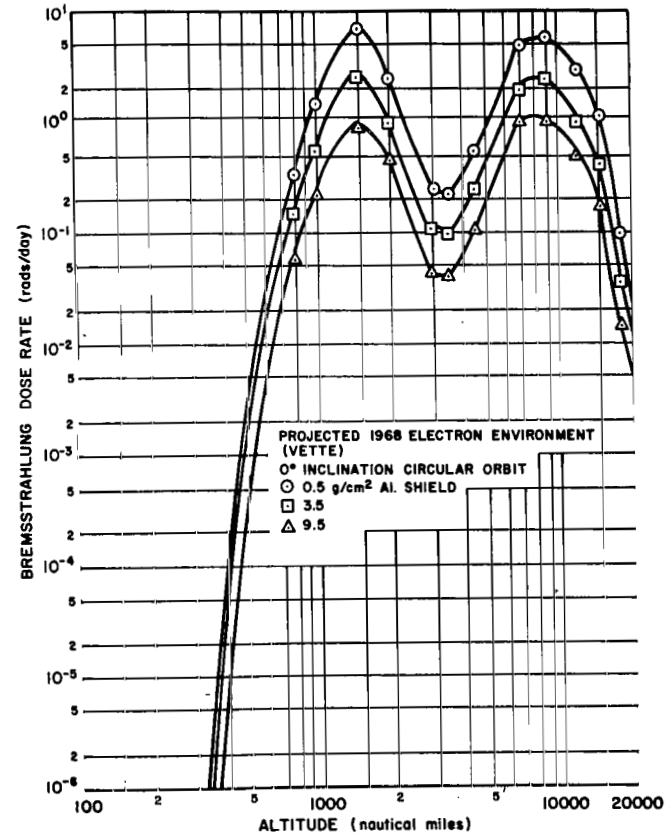
COMPARISON OF ORBITAL INTEGRATIONS AT 60° INCLINATION.

COMPARISON OF ORBITAL INTEGRATIONS AT 90° INCLINATION.

FIGURE 29. PROJECTED ELECTRON ENVIRONMENT FOR DECEMBER 1968

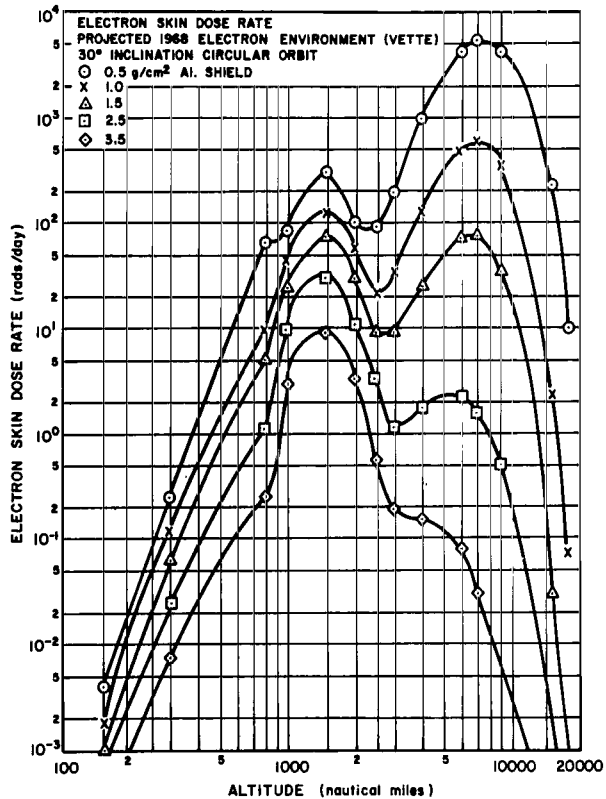


a

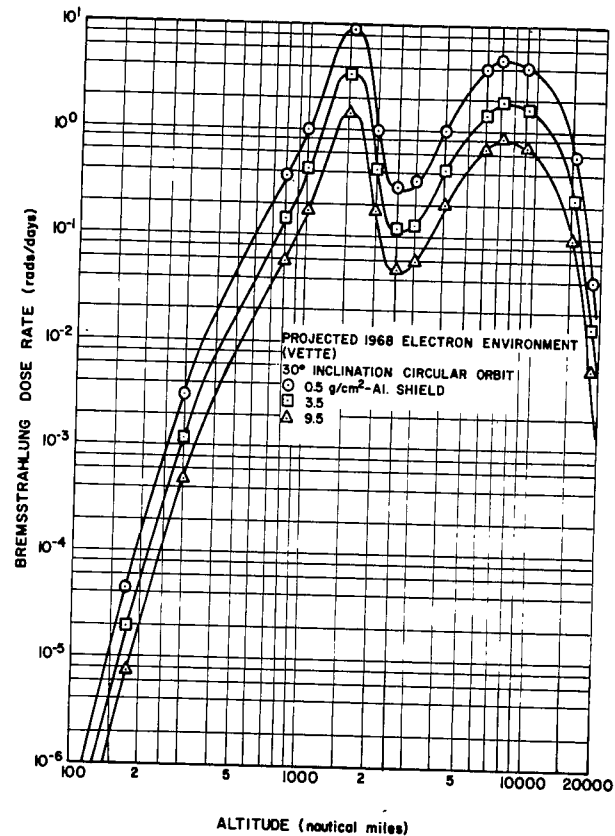


b

FIGURE 30. PROJECTED ELECTRON AND BREMSSTRAHLUNG DOSE RATE AS A FUNCTION OF ALTITUDE AND SHIELD THICKNESS FOR 0-DEGREE ORBITAL INCLINATION

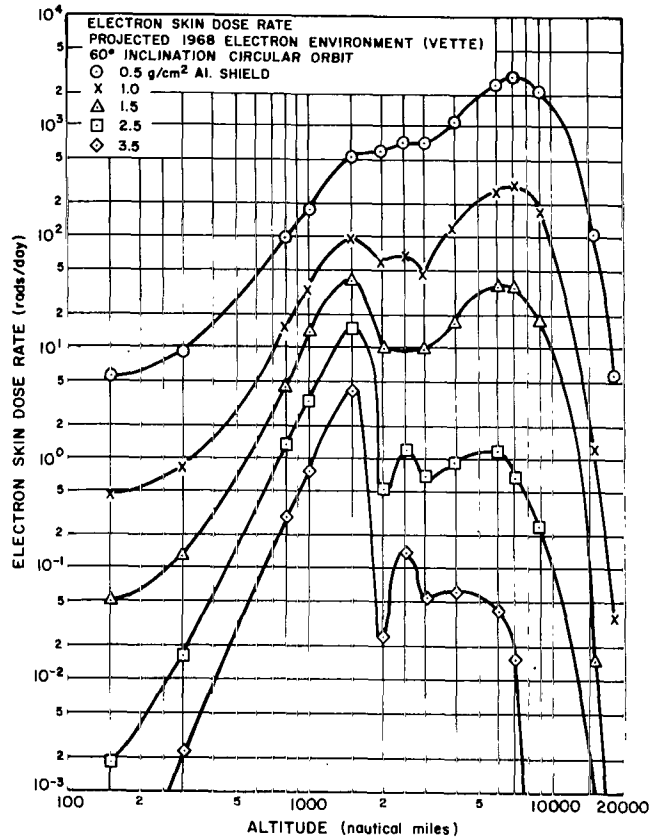


a

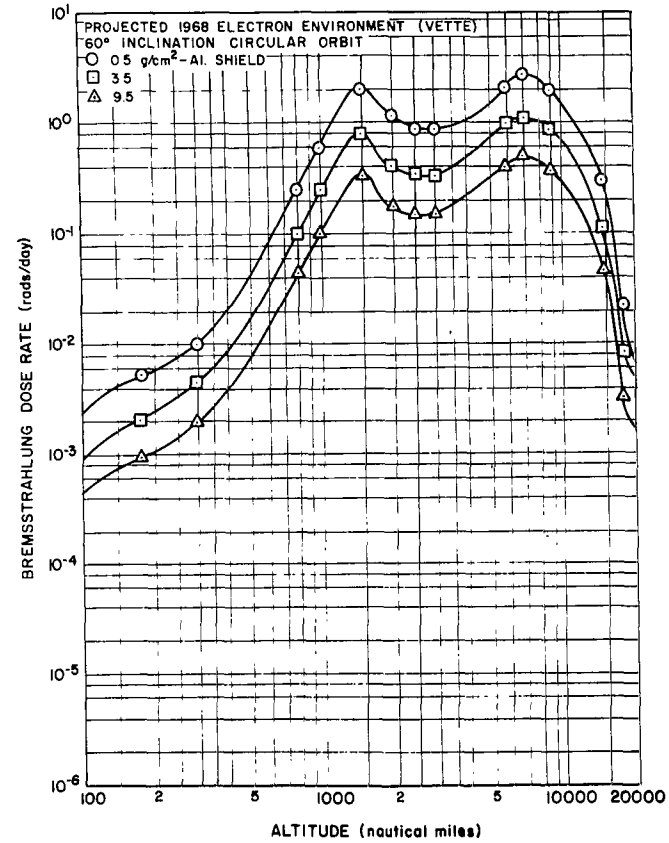


b

FIGURE 31. PROJECTED ELECTRON AND BREMSSTRAHLUNG DOSE RATE AS A FUNCTION OF ALTITUDE AND SHIELD THICKNESS FOR 30-DEGREE ORBITAL INCLINATION

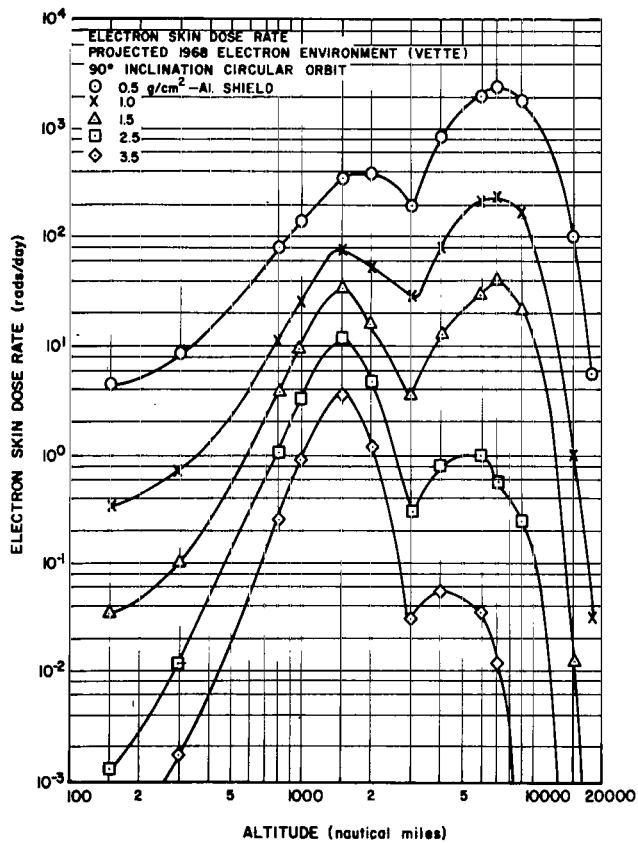


a

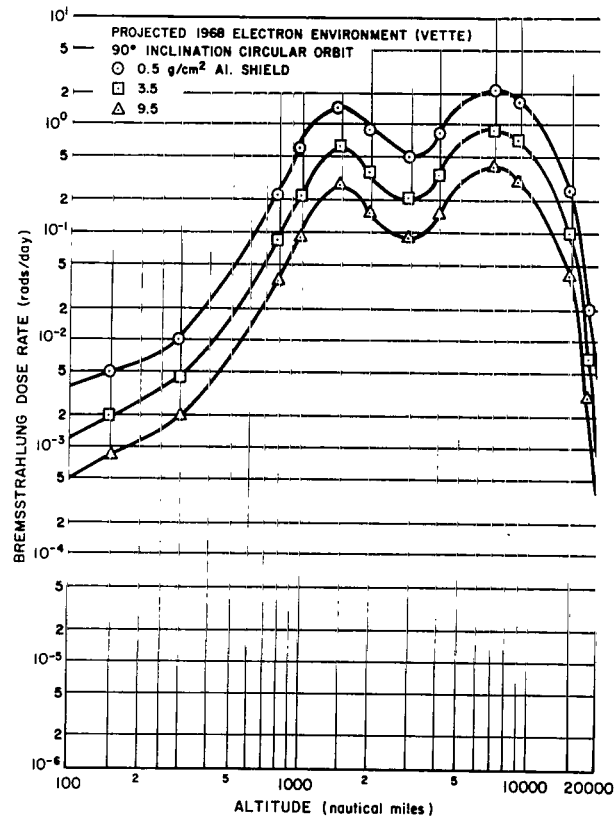


b

FIGURE 32. PROJECTED ELECTRON AND BREMSSTRAHLUNG DOSE RATE AS A FUNCTION OF ALTITUDE AND SHIELD THICKNESS FOR 60-DEGREE ORBITAL INCLINATION



a



b

FIGURE 33. PROJECTED ELECTRON AND BREMSSTRAHLUNG DOSE RATE AS A FUNCTION OF ALTITUDE AND SHIELD THICKNESS FOR 90-DEGREE ORBITAL INCLINATION

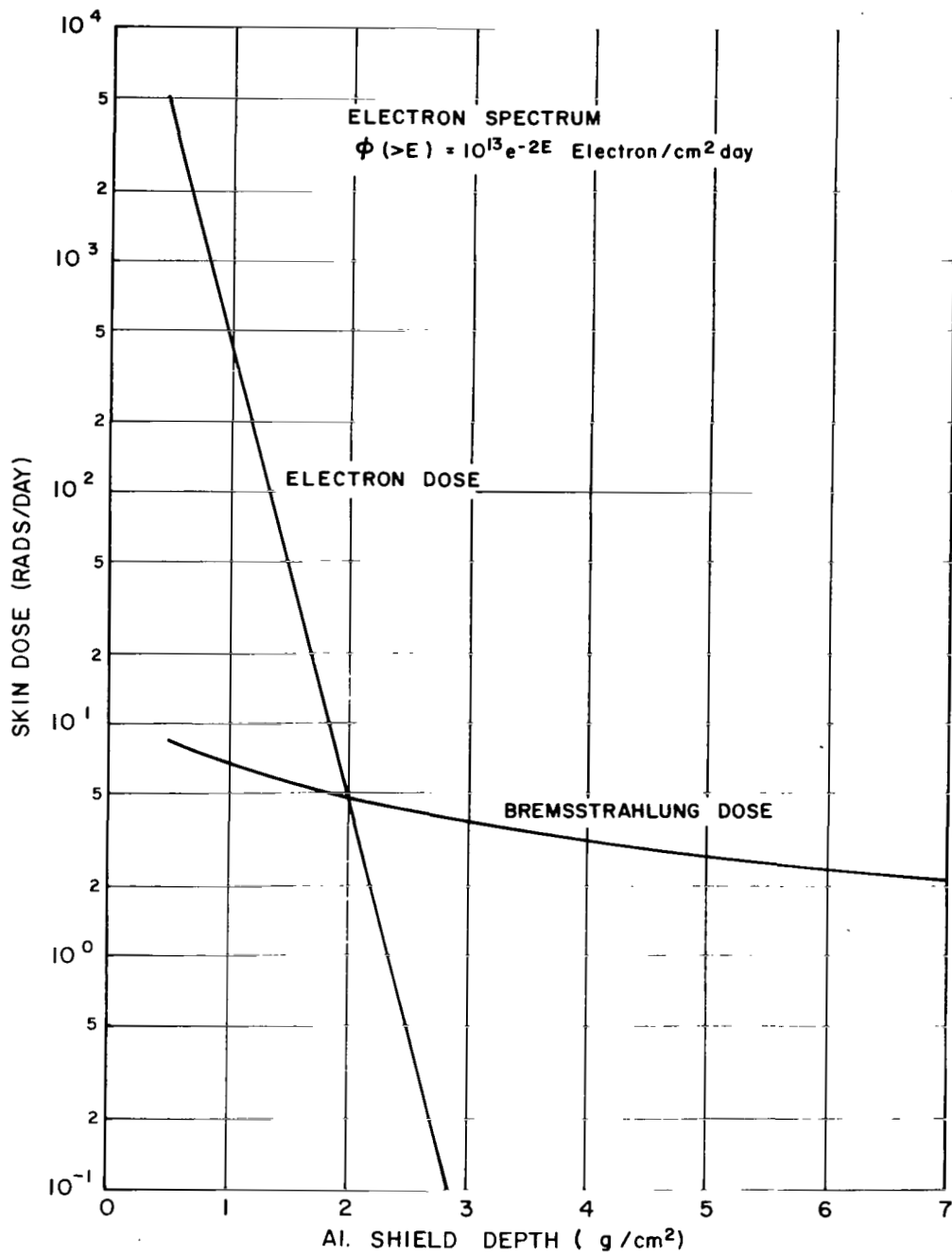
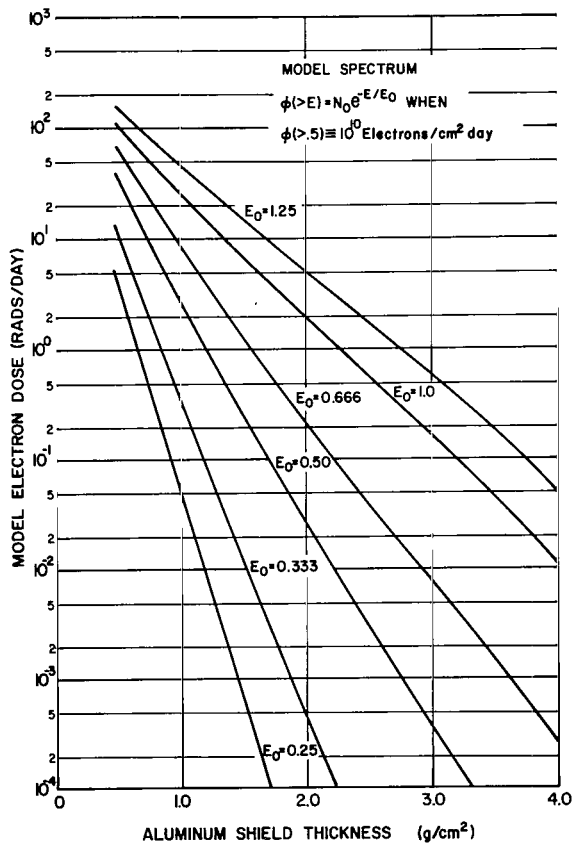
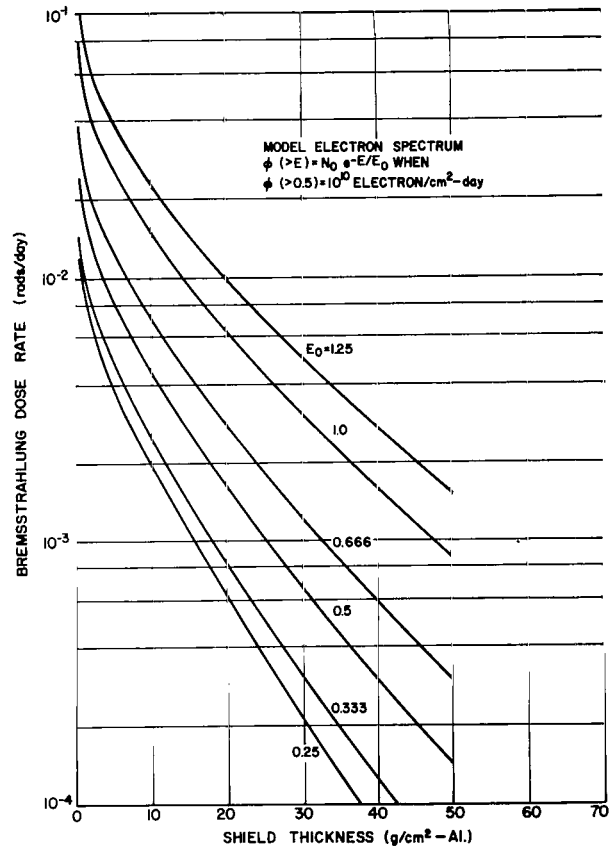


FIGURE 34. ELECTRON AND BREMSSTRAHLUNG DOSE RATE AS A FUNCTION OF SHIELD THICKNESS USING A TYPICAL ELECTRON INTEGRAL SPECTRUM



a



b

FIGURE 35. ELECTRON AND BREMSSTRAHLUNG DOSE RATE AS A FUNCTION OF SHIELD THICKNESS FOR SEVERAL CHARACTERISTIC E_0 VALUES

SYNCHRONOUS ORBIT RADIATION

The galactic cosmic rays, solar flare protons, and trapped electrons are the important dose sources at the synchronous orbit altitude. The dose rates for galactic cosmic rays are shown in Figure 6 of a previous section. The free space dose rate from solar proton events were shown in Figures 9 to 11. Since the vertical cutoff for protons at the synchronous altitude is about 60 MeV, the solar and galactic cosmic ray dose rates will be only slightly modified.

Figure 36 depicts the synchronous orbit electron integral flux as a function of energy and local time as taken from Vette [21]. This electron integral flux is given by the equation

$$\phi(>E, B/B_0, t) = C \cdot A(t) (B/B_0)^{-b} e^{-E/E_0} E^N(t) \frac{\text{electrons}}{\text{cm}^2 \text{sec}} \quad (13)$$

where

$$C = 9 \times 10^7 \text{ at solar minimum (1/2 this at maximum)}$$

$$b = 0.625$$

$$E_0 = 0.215 \text{ MeV}$$

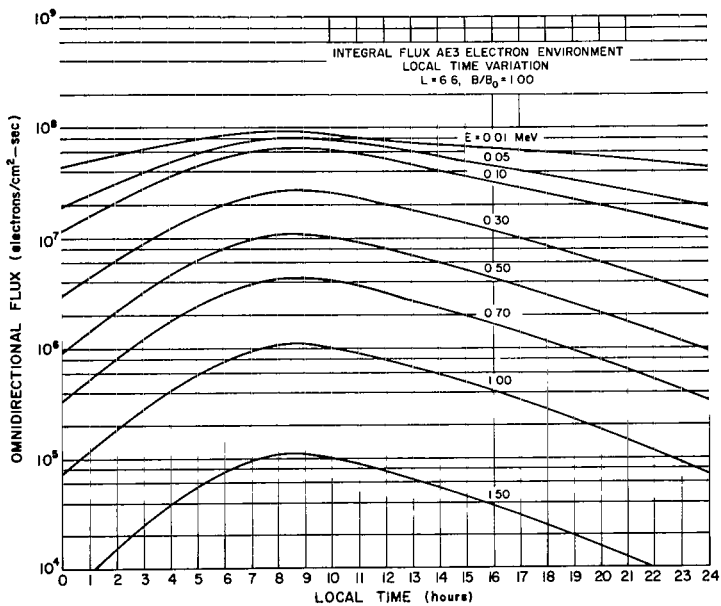
This equation is valid for energies greater than 0.01 MeV. The values of $A(t)$ and $N(t)$ for various local times are given in Reference 21. The values of the above constants at 12:00 noon are $A(t) = 1.00$ and $N(t) = 0.000$.

When the above equation is used, the synchronous altitude electron and bremsstrahlung dose rate as a function of local time and shield thickness would be as shown in Figure 37. The dose rates obtained by integrating over the curves in Figure 37 are shown as curve A of Figure 38.

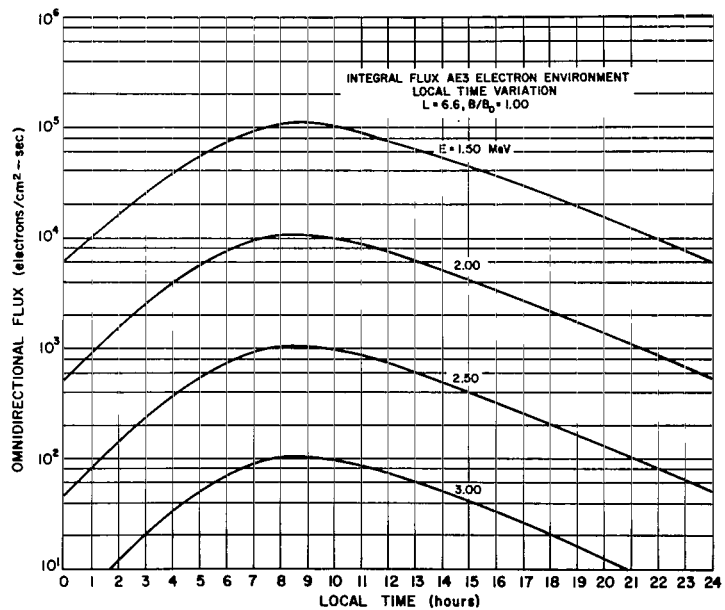
The time average electron integral flux at the equatorial synchronous altitude is given by Vette [21] as

$$\phi(>E) = 5.2 \times 10^7 \exp(-5E) \frac{\text{electrons}}{\text{cm}^2 \text{sec}} \quad (14)$$

The electron dose rate when this average electron spectrum is used is shown as curve B in Figure 38. The bremsstrahlung dose rate is shown as curve C in this figure when the above average flux is used.

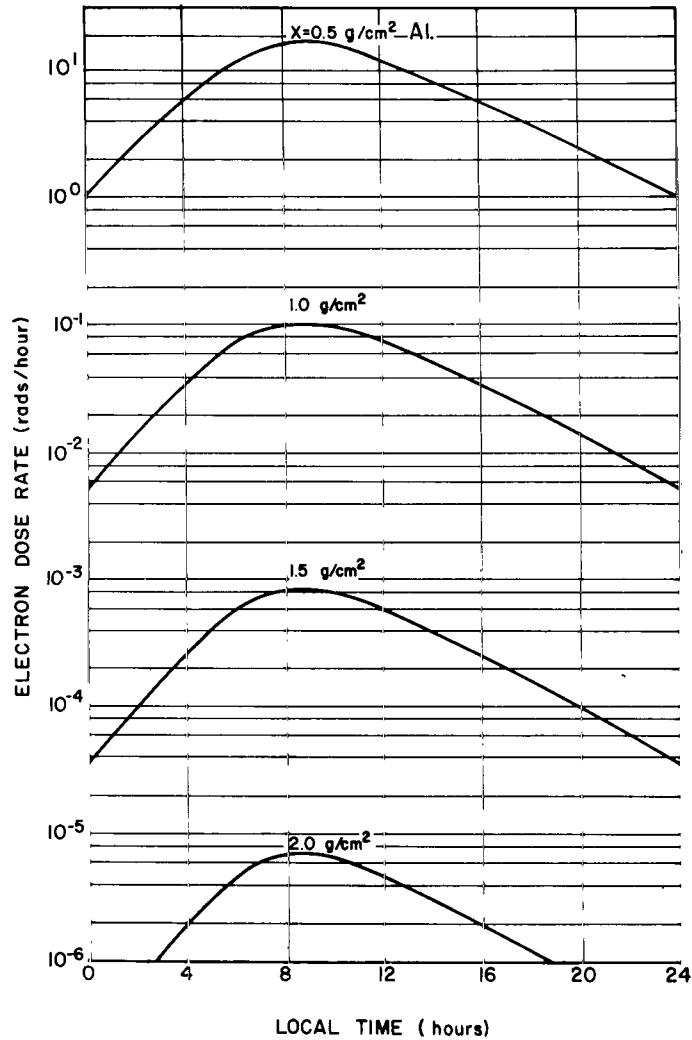


a

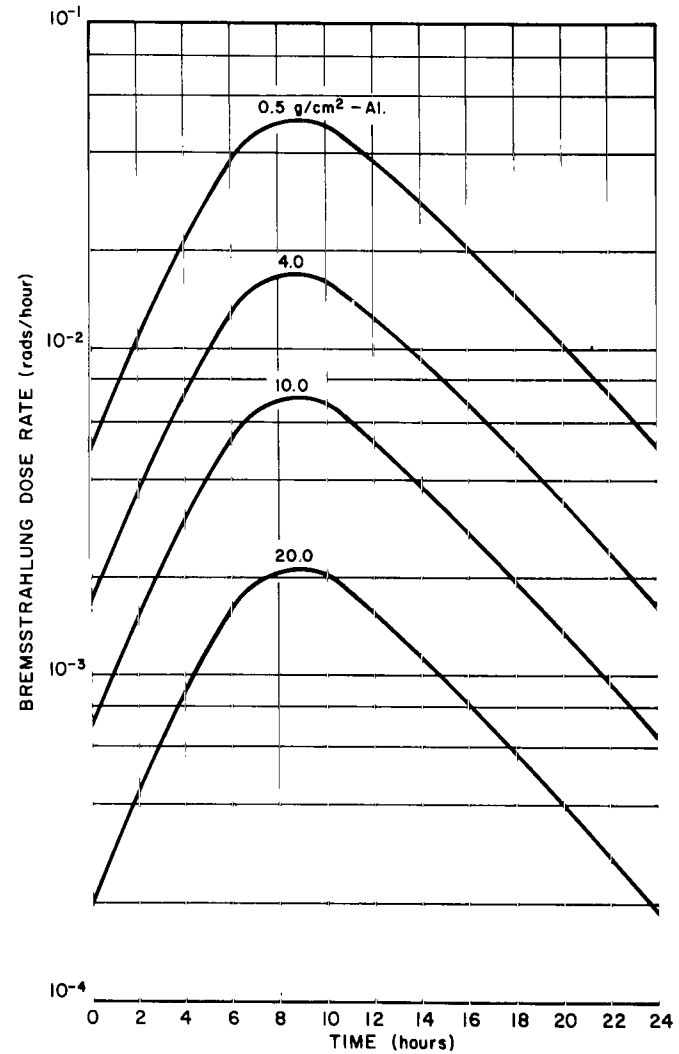


b

FIGURE 36. SYNCHRONOUS ORBIT INTEGRAL ELECTRON FLUX AS A FUNCTION OF LOCAL TIME



a



b

FIGURE 37. SYNCHRONOUS ORBIT ELECTRON AND BREMSSTRAHLUNG DOSE RATE AS A FUNCTION OF SHIELD THICKNESS AND LOCAL TIME

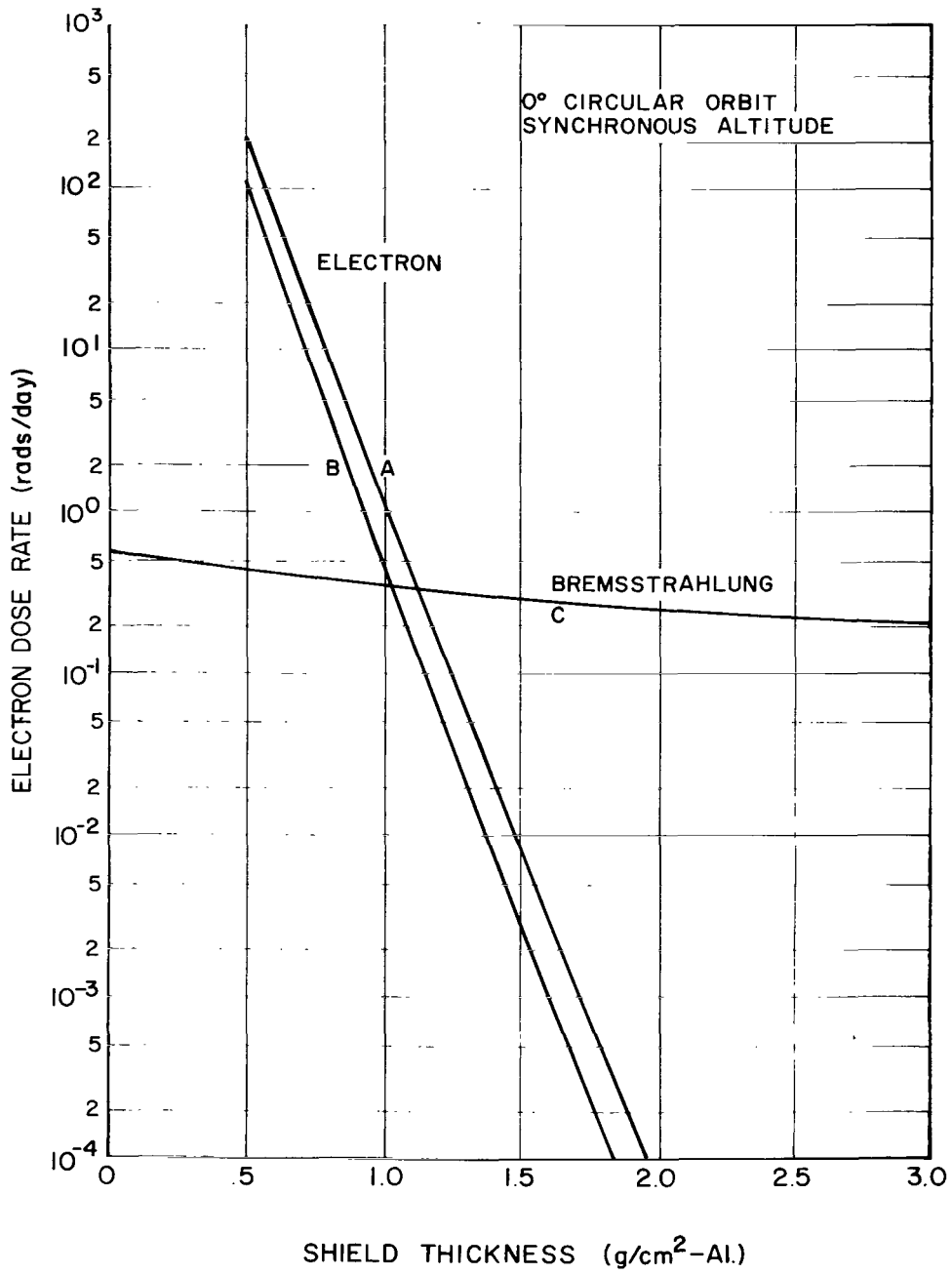


FIGURE 38. SYNCHRONOUS ORBIT ELECTRON AND BREMSSTRAHLUNG DOSE RATE USING AN AVERAGE ELECTRON SPECTRUM

CONCLUSIONS

The results presented in this report should be of practical value for preliminary engineering analysis of space hazards and planning of possible space missions for either near-earth orbits or deep-space probes. The dose rate curves shown in this report are based on the latest available environmental analysis by NASA and the United States Air Force. The environmental models and data will be continually updated as experimental data improve and as more sophisticated analyses are performed. As such modifications become available, the authors of this report intend to update the radiation dose rates in future reports. This is pertinent to the synchronous orbit radiation environment that is now being examined in greater detail by experimental space probes and theoretical analysis.

George C. Marshall Space Flight Center
National Aeronautics and Space Administration
Huntsville, Alabama, November 21, 1967
124-09-11-00-62

APPENDIX

The 1964 electron environmental data, now considered to be out of date, have been placed in the appendix. Figure 39 shows the August 1964 electron flux data as a function of altitude and orbital inclination. The electron and bremsstrahlung dose rates that are shown in Figures 40 and 43 make use of these data.

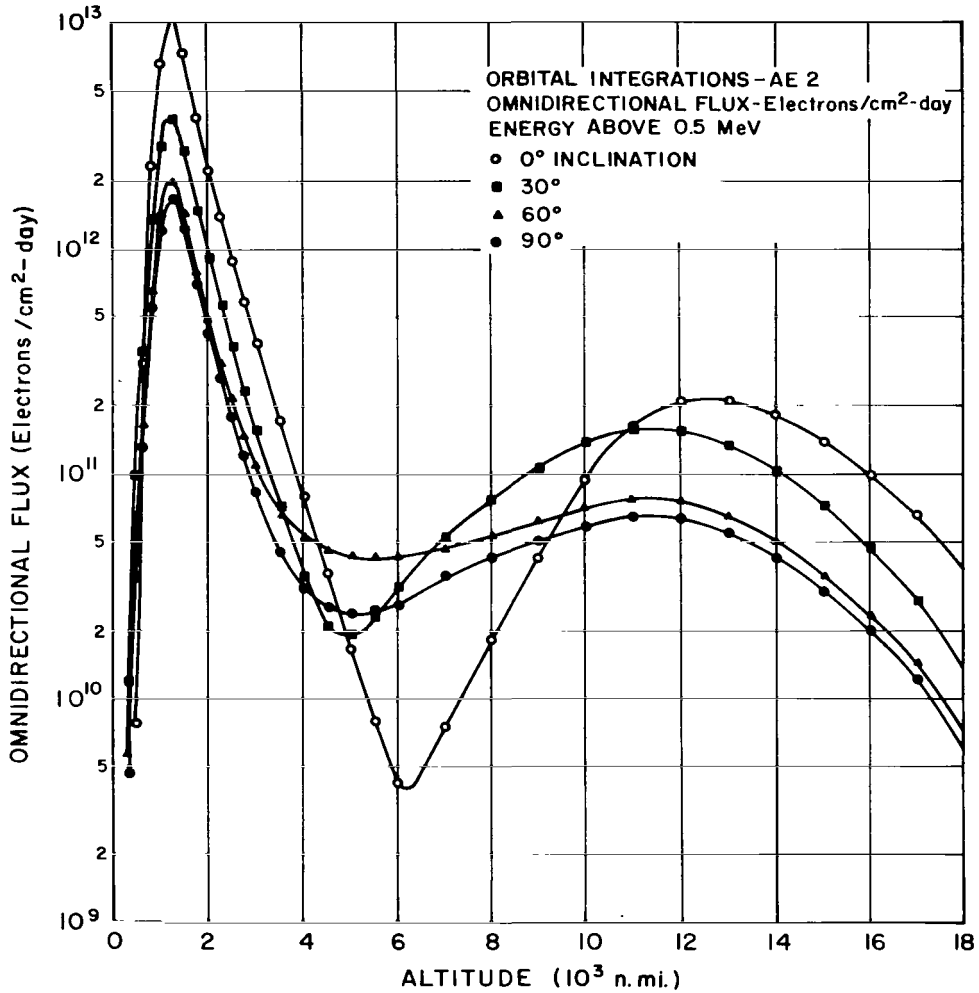
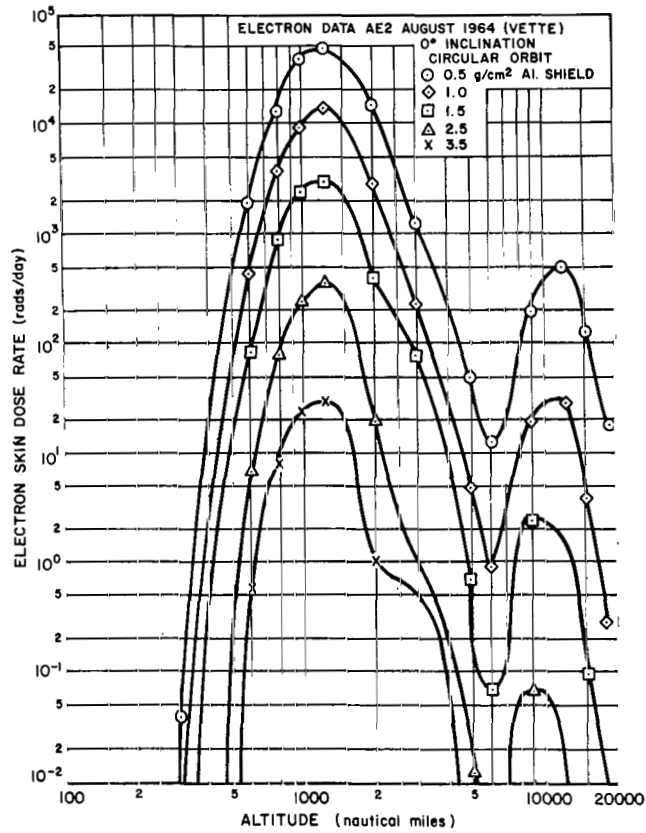
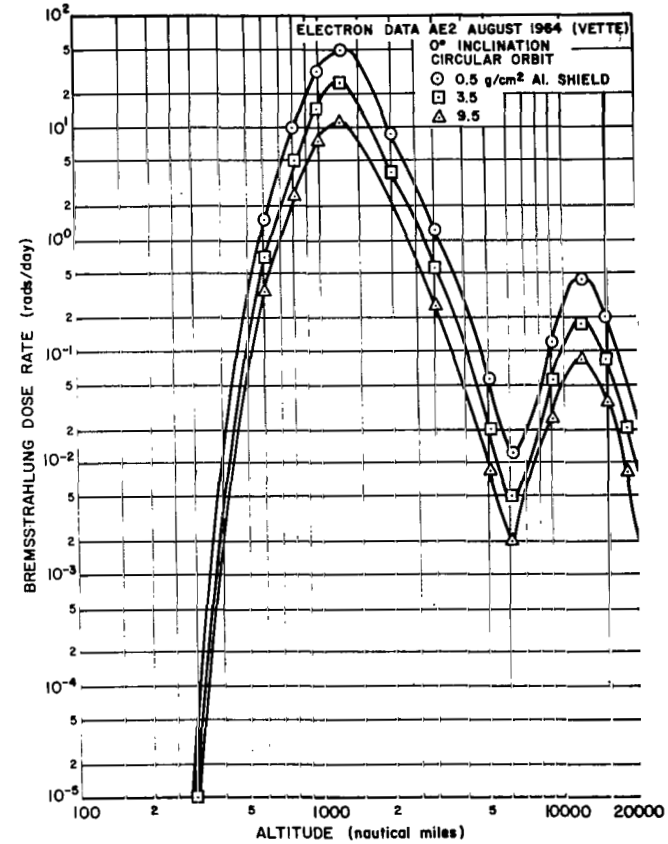


FIGURE 39. TRAPPED ELECTRON FLUX FOR CIRCULAR ORBITS AS A FUNCTION OF ALTITUDE AND ORBITAL INCLINATION

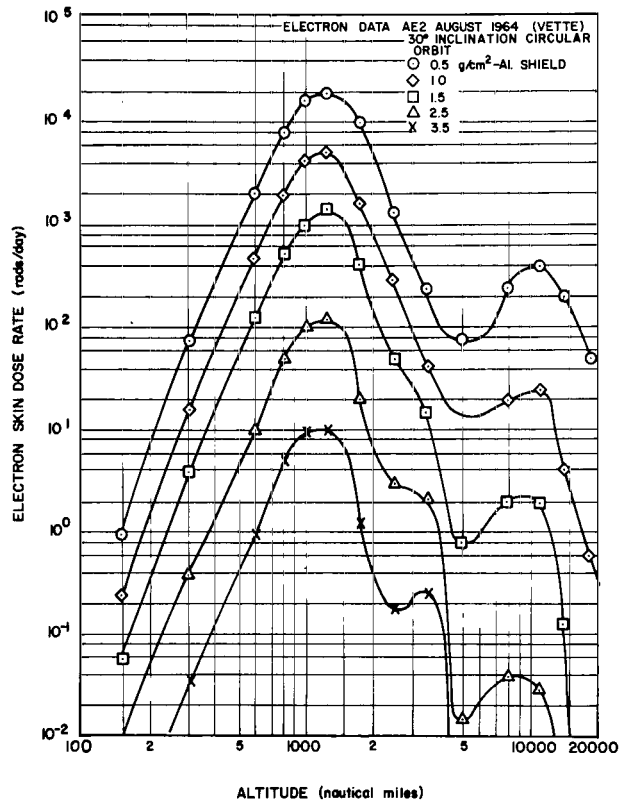


a

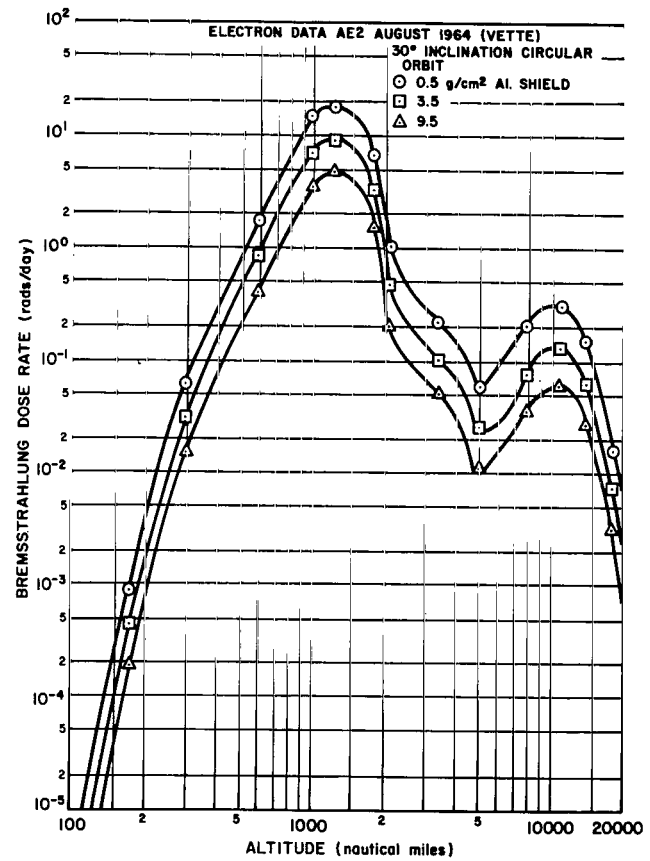


b

FIGURE 40. ELECTRON AND BREMSSTRAHLUNG DOSE RATE AS A FUNCTION OF ALTITUDE AND SHIELD THICKNESS FOR 0-DEGREE ORBITAL INCLINATION

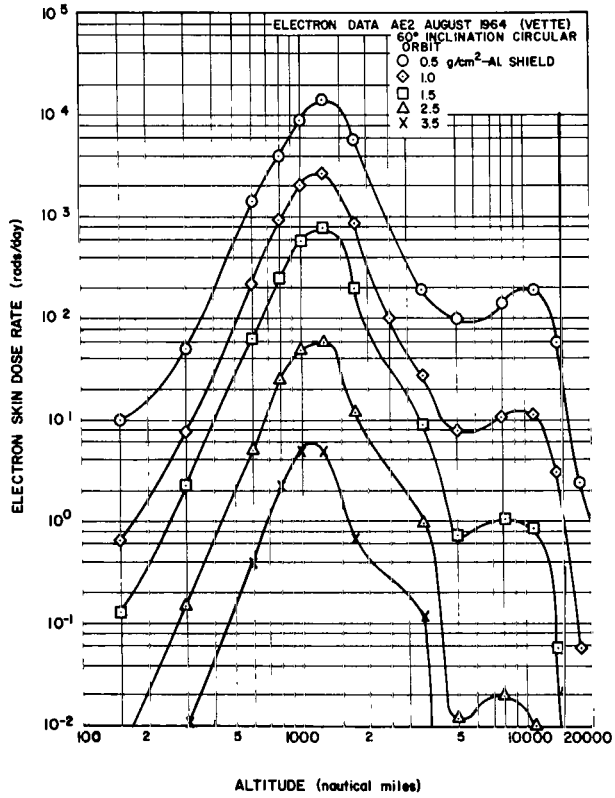


a

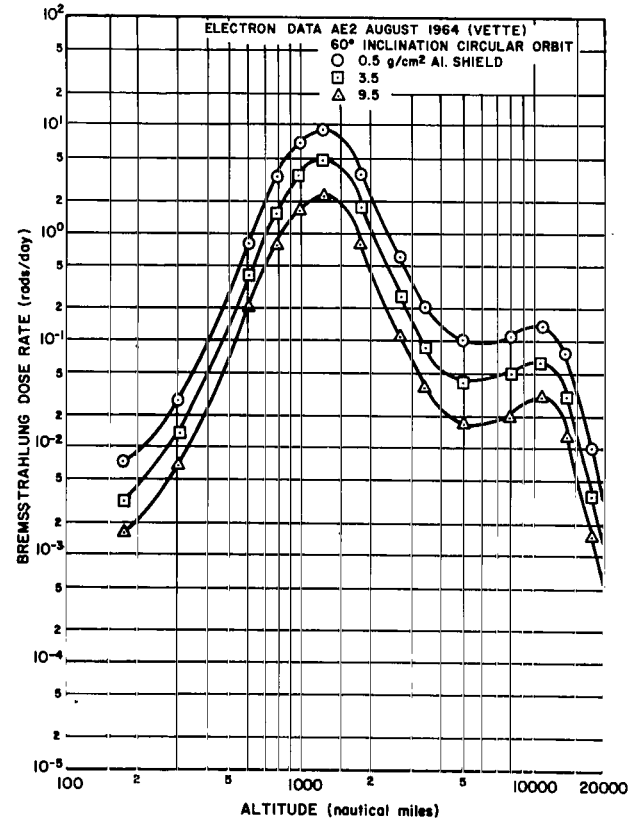


b

FIGURE 41. ELECTRON AND BREMSSTRAHLUNG DOSE RATE AS A FUNCTION OF ALTITUDE AND SHIELD THICKNESS FOR 30-DEGREE ORBITAL INCLINATION

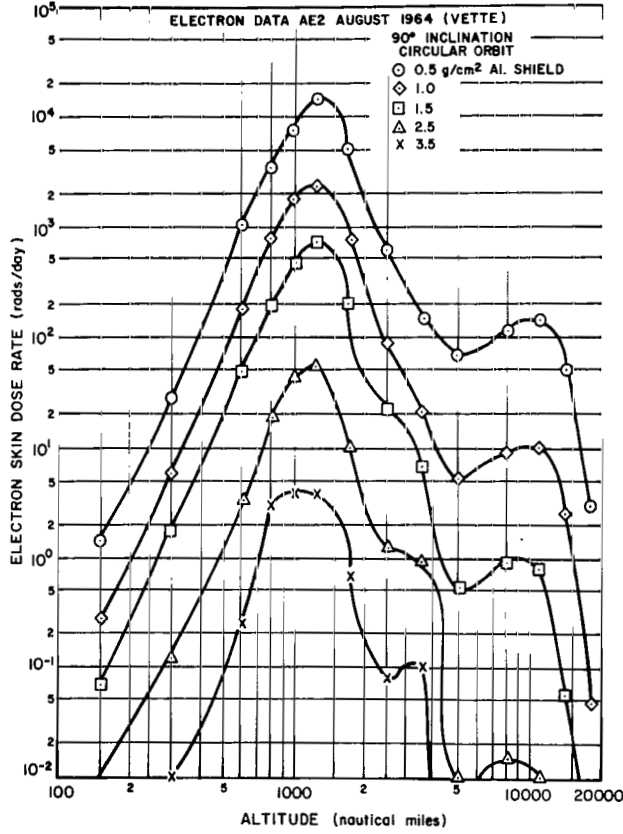


a

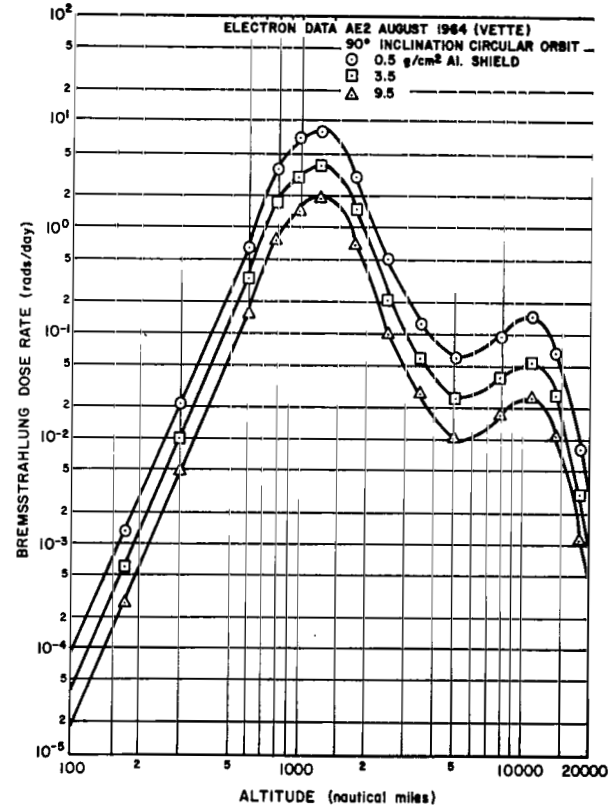


b

FIGURE 42. ELECTRON AND BREMSSTRAHLUNG DOSE RATE AS A FUNCTION OF ALTITUDE AND SHIELD THICKNESS FOR 60-DEGREE ORBITAL INCLINATION



a



b

FIGURE 43. ELECTRON AND BREMSSTRAHLUNG DOSE RATE AS A FUNCTION OF ALTITUDE AND SHIELD THICKNESS FOR 90-DEGREE ORBITAL INCLINATION

REFERENCES

1. Burrell, M. O. : The Calculation of Proton Penetration and Dose Rates. NASA TM X-53063, August 17, 1964.
2. Hilberg, R. H. : Radiation Levels on AS-503 Mission - Case 340, Bellcom, Inc. , July 11, 1966.
3. Coons, D. O. , and Berry, C. A. : Radiation Dose Levels for Apollo Crew Members, Apollo Application Program, File Memorandum to FA/Technical Assistant for Apollo, February 10, 1967.
4. Burrell, M. O. , and Wright, J. J. : The Calculations of Electron and Bremsstrahlung Penetration and Dose Rates. Paper presented at 13th Annual Meeting of the American Nuclear Society, San Diego, California. June 11 - 15, 1967.
5. Ness, N. F. : The Earth's Magnetic Tail. J. Geophys. Res. , vol 70, 1965, p. 2984.
6. McIlwain, C. E. : Coordinates for Mapping the Distribution of Magnetically Trapped Particles. J. Geophys. Res. , vol. 66, no. 11, November 1961.
7. Störmer, C. : Polar Aurora. Oxford University Press, London, 1955.
8. Fermi, E. : Nuclear Physics, Chapter X. University of Chicago Press, Chicago, 1949.
9. Benbrook, J. R. ; Doherty, W. R. ; Sheldon, W. R. ; and Thomas, J. R. : Computer Codes for Space Radiation Environment and Shielding. Report WL TDR-64-71, Vol I, Section 3, The Boeing Company, August 1964.
10. Kuhn, E. ; Payne, W. T. , and Schwamb, F. E. : Solar Flare Hazard to Earth-Orbiting Vehicles. RAC 1395-1, PCD-TR-64-12, Republic Aviation Corporation, July 28, 1964.
11. Balasubrahmanyam, V. K. ; Hagge, D. E. ; Lubwig, G. H. , and McDonald, F. B. : The Multiply-Charged Primary Cosmic Radiation at Solar Minimum, 1965, X-611-65-480, Goddard Space Flight Center, November 1965.

REFERENCES (Concluded)

12. Webber, W. R. : An Evaluation of the Radiation Hazard Due to Solar Particle Events. Document D2-90469, The Boeing Company, December 1963.
13. Baker, M. B. : Geomagnetically Trapped Radiation. Rep. SM-47635, Douglas Aircraft Corporation, October 1964.
14. Hill, C. W. ; Ritchie, W. B. , and Simpson, K. M. : Data Compilation and Evaluation of Space Shielding Problems. Vol. 3, Rep. ER7777, Lockheed Company, April 1966.
15. Webber, W. R. : An Evaluation of Solar Cosmic Ray Events During Solar Minimum. Document D2-84274-1, The Boeing Company, June 1966.
16. Guss, D. E. : Distribution in Heliographic Longitude of Flares Which Produce Energetic Solar Particles. Phys. Rev. Letters, vol. 13, 1964, p. 363.
17. Weddell, J. B. ; Haffner, J. W. , and Morin, F. J. : Statistical Evaluation of Proton Radiation from Solar Flares. Rep. SIB 66-421, North American Aviation, Incorporated, May 20, 1966.
18. Webber, W. R. , and Thomas, J. R. : Sunspot Number and Solar Cosmic Ray Predictions for Cycle 20 (1965 - 1975) With Preliminary Estimates for Cycle 21. Boeing Report D2-113522-1.
19. Norman, J. E. : Estimation of Radiation Hazard Probabilities Due to Solar Proton Events During the Maximum Solar Cycle Phase. Summary Progress Report SSL-27548-1. Research Laboratories, Brown Engineering Company, Incorporated, Huntsville, Alabama, August 31, 1967.
20. Vette, J. I. , et al. : Models of the Trapped Radiation Environment. Vols. 1 and 2, NASA SP-3024, 1966.
21. Vette, J. I. , et al. : Models of the Trapped Radiation Environment. Vol. 3, NASA SP-3024, 1967.
22. Bostrom, C. O. ; Williams, D. J. , and Beall, D. S. : Time Decay of the Artificial Radiation Belt. Trans. Am. Geophys. Union, Vol. 46, 1965, p. 137.

POSTMASTER: If Undeliverable (Section 158
Postal Manual) Do Not Return

"The aeronautical and space activities of the United States shall be conducted so as to contribute . . . to the expansion of human knowledge of phenomena in the atmosphere and space. The Administration shall provide for the widest practicable and appropriate dissemination of information concerning its activities and the results thereof."

—NATIONAL AERONAUTICS AND SPACE ACT OF 1958

NASA SCIENTIFIC AND TECHNICAL PUBLICATIONS

TECHNICAL REPORTS: Scientific and technical information considered important, complete, and a lasting contribution to existing knowledge.

TECHNICAL NOTES: Information less broad in scope but nevertheless of importance as a contribution to existing knowledge.

TECHNICAL MEMORANDUMS: Information receiving limited distribution because of preliminary data, security classification, or other reasons.

CONTRACTOR REPORTS: Scientific and technical information generated under a NASA contract or grant and considered an important contribution to existing knowledge.

TECHNICAL TRANSLATIONS: Information published in a foreign language considered to merit NASA distribution in English.

SPECIAL PUBLICATIONS: Information derived from or of value to NASA activities. Publications include conference proceedings, monographs, data compilations, handbooks, sourcebooks, and special bibliographies.

TECHNOLOGY UTILIZATION PUBLICATIONS: Information on technology used by NASA that may be of particular interest in commercial and other non-aerospace applications. Publications include Tech Briefs, Technology Utilization Reports and Notes, and Technology Surveys.

Details on the availability of these publications may be obtained from:

SCIENTIFIC AND TECHNICAL INFORMATION DIVISION
NATIONAL AERONAUTICS AND SPACE ADMINISTRATION

Washington, D.C. 20546